**African dust transported to Barbados in the Wintertime Lacks Indicators of Chemical Aging**

Haley M. Royer[1,2], Michael T. Sheridan[1,3], Hope E. Elliott[4], Edmund Blades[1], Nurun Nahar

Lata[5], Zezhen Cheng[5], Swarup China[5], Zihua Zhu[5], Andrew P. Ault[6], Cassandra J. Gaston[1*]

[1]Department of Atmospheric Sciences, Rosenstiel School of Marine, Atmospheric, and Earth

Science, University of Miami, Miami, FL, USA

[2]Currently at: Department of Environmental Sciences and Engineering, University of North

Carolina at Chapel Hill, Chapel Hill, NC, USA

[3]Skidaway Institute of Oceanography, University of Georgia, Athens, GA, USA

[4]Department of Ocean Sciences, Rosenstiel School of Marine, Atmospheric, and Earth Science,

University of Miami, Miami, FL, USA

[5]Environmental Molecular Sciences Laboratory, Pacific Northwest National Laboratory,

Richland, WA, USA

[6]Department of Chemistry, University of Michigan, Ann Arbor, MI, USA

*Corresponding Author:

Cassandra J. Gaston: Email: cgaston@miami.edu, Phone: (305)-421-4979

26 **Abstract**

27 The chemical processing ("aging") of mineral dust is thought to increase dust light scattering

28 efficiency, cloud droplet activation, and nutrient solubility. However, the extent of African dust

29 aging during long-range transport to the western Atlantic is poorly understood. Here, we explore

30 African dust aging in wintertime samples collected from Barbados when dust is transported at

31 lower altitudes. Ion chromatography (IC) analysis indicates that the mass concentrations of bulk

32 nitrate, sulfate, and oxalate increase, relative to background conditions, when African dust

33 reaches Barbados after transatlantic transport, indicating dust aging. However, aerosol mixing

34 state analysis from computer-controlled scanning electron microscopy with energy dispersive x-

35 ray spectroscopy (CCSEM/EDX) indicates that approximately 67% of dust particles are

36 internally mixed with sea salt, while only about 26% of dust particles contain no internally mixed

37 components. SEM/EDX elemental mapping and time-of-flight secondary ion mass spectrometry

38 (TOF-SIMS) reveals that within internally mixed dust and sea salt particles, only sea salt

39 components contain signs of aging as indicated by the loss of chloride and acquisition of nitrate

40 and/or sulfate. Our results suggest that chemical aging may only modestly increase the solubility

41 of nutrients in African dust during long range transport. Because most dust that we measured was

42 internally mixed with sea salt, chemical aging is not necessarily required to increase the

43 hygroscopicity of dust, at least in the lower boundary layer. Further, our findings have

44 implications for understanding the release of halogens from sea salts, which may be enhanced in

45 internally mixed dust and sea salt particles.

46

47

48

**1. Introduction**

Upon emission, dust can directly scatter or absorb solar radiation (Balkanski et al., 2007; Haywood et al., 2003; Myhre & Stordal, 2001; Sokolik et al., 2001; Tegen, 2003), act as cloud condensation (Albrecht, 1989; Koehler et al., 2009; Levin et al., 1996; Rosenfeld et al., 2001) and ice nuclei (Archuleta et al., 2005; Cziczo et al., 2004; DeMott et al., 2003), and provide micro- and macro- nutrients to nutrient-limited ecosystems (Elliott et al., 2024; Jickells et al., 2005; Mahowald, 2011). However, mineral dust aerosol is still poorly represented in climate models due, in part, to a lack of understanding of the physiochemical properties of dust and their changes as a result of cloud processing (Gierlus et al., 2012; Wurzler et al., 2000), multiphase reactions (Andreae et al., 1986; Sullivan et al., 2007; Sullivan & Prather, 2007) or heterogeneous reactions with polluted air masses (Fitzgerald et al., 2015; Krueger et al., 2004; Sullivan et al., 2009). The chemical change in the physiochemical properties of dust due to heterogeneous or multiphase reactions, herein referred to as "aging", can alter the water uptake properties of dust (Krueger et al., 2003; Laskin et al., 2005) thus affecting its light scattering efficiency (Bauer et al., 2007; Kandler et al., 2011; Levin et al., 1996), cloud droplet activation properties (Gibson et al., 2007; Kelly et al., 2007; Sullivan et al., 2009; Tang et al., 2016), and atmospheric lifetime (Abdelkader et al., 2015; Lance et al., 2013; Li et al., 2014; Wu et al., 2013). We note that chemical aging is distinct from other changes in the physicochemical properties of dust that may occur during transport such as coagulation. Chemical aging is also essential to increase the bioavailability of nutrients within dust via ligand-mediated and proton-mediated dissolution processes (Nenes et al., 2011; Spokes & Jickells, 1995; Stockdale et al., 2016). Modeling the chemical aging process is challenging and, as a result, models often treat dust as a chemically

71    homogeneous and hydrophobic particle type (Han et al., 2011; Pringle et al., 2010; Shi et al.,

72    2008), which oversimplifies the complexity of dust and its impacts in the atmosphere.

73        African dust is the largest source of dust, which is transported to the Caribbean, North

74    and South America and Europe (Barkley et al., 2019; Prospero & Mayol-Bracero, 2013). Most

75    research studying African dust transport focuses on the summer when dust mass concentrations

76    are at a maximum (Prospero & Mayol-Bracero, 2013; Zuidema et al., 2019) and the Saharan Air

77    Layer (SAL) that transports dust across the Atlantic is at its maximum altitude (Carlson &

78    Prospero, 1972). The height of African dust transport minimizes the mixing time of transported

79    dust with the underlying Marine Boundary Layer (MBL) until the dust settles out of the SAL

80    (Ryder et al., 2018). Studies exploring African dust aging during the summertime have produced

81    varying results. Early attempts to study dust aging in the western Atlantic from Li-Jones &

82    Prospero, 1998, found a strong correlation between mineral dust and non-sea salt sulfate (NSS-

83    $SO_4^{2-}$) from size-resolved filter measurements collected in Barbados during the boreal spring,

84    which they conclude is the result of dust aging by sulfur emissions from Europe. In a more recent

85    study from Izaña, African dust has been shown to acquire sulfate from industrial emissions from

86    North Africa (Rodriguez et al., 2011). Further, single-particle methods have been utilized to

87    obtain more detail on the mixing state of dust to unambiguously determine if markers of aging

88    are located within dust or other aerosol particles. Conclusions from Denjean et al., 2015, inferred

89    from low hygroscopicity growth measurements, that long range transported  African dust

90    particles collected over Puerto Rico in the boreal summer are not chemically processed and are

91    minimally mixed with other chemical components. In contrast, iron solubility was found to

92    increase in Saharan dust during transatlantic transport, in part, due to chemical aging (Rodriguez

93    et al, 2021). Further, Fitzgerald et al., 2015 also analyzed long range transported African dust in

Puerto Rico during the boreal summer, but found sulfate and oxalate on dust particles using real-time single-particle mass spectrometry. Dust composition measured by Fitzgerald et al., 2015 may have also been affected by local cloud processing as sampling occurred within a cloud forest. Boreal summer analysis of long range transported dust in Barbados from Kandler et al., 2018 and Weinzierl et al., 2017 revealed limited aging of dust particles with some internal mixing with other chemical components from microscopy and spectroscopy analysis. Model analysis of summertime African dust transport from Abdelkader et al., 2017 explored the evolution of dust aging as dust is transported from Africa to the western Atlantic, finding that aged African dust is quickly removed from the aerosol loading during transit across the Atlantic, leaving minimally-aged dust within the aerosol loading that reaches the western Atlantic.

Unlike the summertime when dust is transported within the elevated SAL, dust is transported at lower altitudes during the wintertime (Tsamalis et al., 2013) enhancing the mixing time of dust within the MBL, which may increase the interaction between dust, anthropogenic emissions, and marine biogenic emissions in the MBL (Gutleben et al., 2022; Savoie & Prospero, 1982). In addition to anthropogenic emissions that mix with dust (Gaston et al., 2024; Rodriguez et al., 2011), the Sahelian burn season occurs during the boreal winter, often resulting in long-range co-transport of dust and smoke emissions that were specifically observed during the ATOMIC/EUREC[4]A campaigns (Quinn et al., 2021; Royer et al., 2023). Smoke emissions are known to contain sulfur dioxide ($SO_2$) and nitrogen oxides (e.g., $NOx \equiv NO + NO_2$) that theoretically could age dust extensively (Hickman et al., 2021; Rickly et al., 2022), especially during long-range transport in which dust has several days to interact with smoke emissions before it arrives in the western Atlantic. During the ATOMIC/EUREC[4]A campaigns, sulfate was observed on smoke particles, indicating a potential for dust aging during co-transport with smoke

117    (Royer et al., 2023). However, the likelihood of mixing between the emissions in the MBL, dust,

118    and African smoke emissions and their impact on dust aging during the wintertime is unclear.

119          The goal of this study is to determine the extent of aging on African dust particles

120    transported to the Caribbean during the boreal winter using methods that determine the mixing

121    state of individual particles. Collection of aerosol samples took place at the Barbados

122    Atmospheric Chemistry Observatory (BACO) at Ragged Point, Barbados from January through

123    February of 2020 during the ATOMIC/EUREC$^4$A campaign. During the sampling period, 3 dust

124    events consisting of co-transported dust and smoke originating from Africa arrived at Barbados,

125    offering ample opportunity to study the extent of aging. Lidar measurements also reveal that

126    dust-laden air masses remained at a low altitude (3.5 km) for the duration of their transit to

127    Ragged Point, contrasting high altitude summertime transport conditions (Gutleben et al., 2022).

128    This study provides a unique opportunity for exploring the extent of dust aging on African dust,

129    which should be at a maximum under the conditions described. Our findings  provide much

130    needed insight into the extent of aging for African aerosols undergoing long range transport to

131    the western Atlantic, which is essential for properly modeling the water uptake properties of dust

132    particles in the atmosphere as well as the solubility of nutrients in dust bearing minerals.

133    **2.  Methods**

134    *2.1 Measurement Site and Sampling Period*

135          The sampling site, sampling period, and air mass origins that were studied have been

136    described previously in Royer et al., 2023. Briefly, aerosol samples consisting of long-range co-

137    transported African dust and smoke as well as marine aerosols were collected at the University

138    of Miami's Barbados Atmospheric Chemistry Observatory (BACO) at Ragged Point during the

139    EUREC$^4$A and ATOMIC campaigns from 20 January through 20 February 2020 (Quinn et al.,

140   2021; Stevens et al., 2021). Air mass origins were determined using NOAA's HYSPLIT model

141   as well as daily dust mass concentrations (Stein et al., 2015). Ragged Point (13°6' N, 59°37'W) ,

142   a prominence on Barbados' eastern coast, is an ideal location for studying the extent of dust

143   aging in long range transported African aerosols as it is exposed to the steady easterly trade

144   winds which regularly carry outflows of African aerosols such as dust and smoke to the island

145   (Archibald et al., 2015; Carlson & Prospero, 1972; Prospero, 1968) and minimize the influence

146   of anthropogenic activity from local islands to the west (Prospero et al., 2005; Savoie et al.,

147   2002).

148          In this study, we utilize both bulk and single-particle methods to highlight the importance

149   of aerosol mixing state for understanding the extent of dust aging. Bulk methods have

150   traditionally been used to study long-range dust transport and the extent of dust aging in the

151   western Atlantic (Chen & Siefert, 2004; Li-Jones & Prospero, 1998; Savoie et al., 2002). Single

152   particle methods used herein show that elucidating the aerosol mixing state is essential for

153   determining the full extent of aging in long range transported African dust particles.

154   *2.2 Mass Concentrations of Dust and Soluble Ion Content*

155          To collect aerosol samples, the BACO is equipped with a high-volume sampler and an

156   isokinetic aerosol inlet on top of a 17 m-tall tower situated on a 30 m bluff along the coast at

157   Ragged Point. Aerosol filters were collected using a high-volume sampler pumping at a rate of

158   approximately 0.7 $m^3$/min for bulk measurements and 1.0 $m^3$/min for size-resolved

159   measurements. Size-resolved filters were collected on a cascade impactor (Tisch Environmental,

160   Inc., Series 230) with 6 stages and 1 backing filter. Size-resolved aerosol analysis are separated

161   into supermicron (stages 1-4; >1.3 μm) and submicron (stages 5 – backing filter; <1.3 μm). All

162   aerosol filter samples were collected on cellulose Whatman-41 (W-41) filters with a nominal 20

163     μm pore size. After filter collection, filters were washed with Milli-Q water three times to

164     remove soluble material. The washed filters were subsequently combusted in a furnace at 500 °C

165     for about 12 h (i.e., overnight) to remove the cellulose filter and determine daily dust mass

166     concentrations (Prospero et al., 2021; Zuidema et al., 2019). Procedural filter blanks were also

167     collected by placing a filter in the sampler cassette for 15 min without turning on the pump. The

168     resulting ash mass from a sample minus the mass of a filter blank is the gross ash weight, which

169     is then adjusted by a factor of 1.3 to convert the ash weight to a mineral dust concentration

170     (Prospero, 1999; Zuidema et al., 2019).

171         To determine daily bulk and size-resolved soluble ion content, the 20 mL of Milli-Q used

172     to wash the filters was filtered through a 25 mm membrane filter with 0.4 μm pore size

173     (Whatman Nuclepore Track Etch Membrane) to remove any particulates from the washing

174     process. Filtrate was then frozen in a -20°C freezer until analysis. To prepare samples, frozen

175     filtrate was thawed in a warm water bath and vortexed for 20 sec. The filtrate was then analyzed

176     using an ion chromatography (IC) instrument (Dionex Integrion HPIC System; Thermo

177     Scientific). Samples were analyzed in triplicate to ensure precision of results. To obtain soluble

178     ion content, 5 mL aliquots of filtrate were injected into the IC system and analyzed for cations

179     (IonPac CG12A/CS12A; Thermo Scientific) and anions (IonPac AS11-HC; Thermo Scientific).

180     Cations of interest analyzed by IC include lithium ($Li^+$), sodium ($Na^+$), ammonium ($NH_4^+$),

181     potassium ($K^+$), magnesium ($Mg^+$), and calcium ($Ca^+$) while anions of interest include fluoride

182     ($F^-$), formate ($CH_2O^-$) , methanesulfonate (MSA), chloride ($Cl^-$), nitrite ($NO_2^-$), bromide ($Br^-$),

183     nitrate ($NO_3^-$), sulfate ($SO_4^{2-}$), oxalate, and phosphate ($PO_4^{3-}$). Since the filtrate analyzed includes

184     sea salt emissions, which may include sulfate from ocean emissions, non-sea salt sulfate (NSS-

185     $SO_4^{2-}$) was calculated using the equation (Gaston et al., 2024)

186     $[NSS - SO_4^{2-}] = [SO_4^{2-}] - (0.2517 * [Na])$                          (1)

187     to determine the fraction of sulfate derived from non-sea spray emissions including

188     anthropogenic and marine biogenic sources. For the purposes of this study, we focus primarily

189     on NSS-$SO_4^{2-}$ and $NO_3^-$ as they are chemical indicators of dust aging (Sullivan et al., 2007) as

190     well as oxalate as it indicates cloud processing and other processes (Ma et al., 2004). Samples

191     were also analyzed for methanesulfonate, an important tracer of ocean-derived biogenic sulfur

192     (Gaston et al., 2010) that can age dust particles (Desboeufs et al., 2024), however MSA

193     measurements were negligible.

194     *2.3 Aerosol Collection for Single Particle Mixing State Analysis*

195        To determine the mixing state of individual particles, aerosol samples were collected at

196     ambient relative humidity (RH) through an isokinetic aerosol inlet with a three-stage

197     microanalysis particle sampler (MPS-3, California Measurements, Inc.), which samples particles

198     from diameters of 5.0-2.5 μm (stage 1), 2.5-0.7 μm (stage 2), and <0.7 μm (stage 3). For each set

199     of samples (one set including one sample from each stage of the MPS), the MPS was run for 45

200     min at 2 L/min flow starting at approximately 09:30 LT (local time) or 13:30 coordinated

201     universal time (UTC). Meteorological data from a local station were used to manually check that

202     wind direction fell between 335 and 130 degrees and that wind speeds were greater than 1 m/s

203     during all sampling periods to ensure that only air from the open ocean to the east was sampled

204     rather than local, anthropogenically-influenced air.

205     *2.4 Single Particle Elemental Composition and Particle Source Determined from Computer*

206     *Controlled Scanning Electron Microscopy Coupled to Energy Dispersive X-ray Spectroscopy*

207     *(CCSEM-EDX)*

208    To determine aerosol elemental composition, particles were deposited onto carbon-coated

209    copper grids (Ted Pella, Inc., Prod. # 01910-F) on each of the 3 stages of the MPS that were later

210    analyzed at the Environmental Molecular Science Laboratory (EMSL) at Pacific Northwest

211    National Laboratory (PNNL) using computer-controlled scanning electron microscopy (Quanta

212    3D) coupled with energy-disperive X-ray spectroscopy (EDAX, Inc.) (CCSEM/EDX). SEM

213    provides images, size, and morphology of individual particles while EDX measures the semi-

214    quantitative elemental composition of each particle. Approximately 1800 particles from stage 1,

215    2500 particles from stage 2, and 3200 particles from stage 3 were analyzed via CCSEM/EDX for

216    each day of sampling. Only particles with diameters >0.1 μm were analyzed. Semiquantitative

217    data products from CCSEM/EDX analysis were then analyzed in MATLAB (version 9.6.0; The

218    Mathworks, Inc.) using a k-means clustering algorithm (Ault et al., 2012; Royer et al., 2023;

219    Shen et al., 2016) to group similar particles into clusters based on the elemental percentage, size,

220    and shape of individual particles. These clusters are then assigned to particle types based on their

221    morphology, characteristic EDX spectra, and the existing literature. Percent composition

222    threshold values of 1% were used when processing CCSEM/EDX data to ensure the presence of

223    elements detected by the EDX. Single particle analysis using CCSEM/EDX was limited to 16

224    elements found in common aerosols such as dust, sea salt, and smoke particles: carbon (C),

225    nitrogen (N), oxygen (O), sodium (Na), magnesium (Mg), aluminum (Al), silicon (Si),

226    phosphorus (P), sulfur (S), chlorine (Cl), potassium (K), calcium (Ca), vanadium (V), manganese

227    (Mn), iron (Fe), and nickel (Ni). To prevent the signal from the copper (Cu)-grid from interfering

228    with measuring the other elements in the particles, Cu was intentionally excluded from the list of

229    elements to detect. Though the grids are coated with carbon  (C), C was intentionally included

230    due to the presence of organics within the aerosol loading. The inclusion of C may result in a

231  small underrepresentation of other elements of interest as the C signal may be artificially

232  elevated by the C-coating on the Cu-grids. Commonly used thresholds for detecting an element

233  with CCSEM-EDX are 0.5-1% (by mole fraction) (Hopkins et al., 2008), and depend on factors

234  such as substrate, collection time of spectra, accelerating voltage, sensitivity of the sample to the

235  electron beam, and the element being measured (i.e., EDX is less sensitive to N than S in this

236  analysis). A rough rule of thumb is that when elements are not detected they are < 1% of particle

237  mass.

238       Particle identification was primarily based on semiquantitative elemental composition

239  determined by EDX. Dust particles were identified based on the presence of elements common

240  in aluminosilicate minerals, including Si, Al, Fe, K, Ca, and Mg detected from EDX analysis

241  (Hand et al., 2010; Krueger et al., 2004; Levin et al., 2005). Sea salt particles were characterized

242  by high Na and Cl content, indicating the presence of halite (NaCl) (Bondy et al., 2018). Smoke

243  particles were identified as containing a combination of C, O, S, and K, as shown previously at

244  this site (Royer et al. 2023) and other sites (Bondy et al. 2018; Olson et al. 2019).  Internal

245  mixtures of dust and sea salt contained elements indicative of both dust (Si, Al, Fe, K, Ca, and

246  Mg) and sea salt (Na and Cl), usually with portions of the particle containing primarily dust and

247  other portions containing primarily sea salt. Internally mixed dust and smoke contained elements

248  common in mineral dust as well as high C, K, and S which are representative of carbon-based

249  matter that has undergone combustion and aging from sulfur componds, leading to the formation

250  of potassium-containing salts (Andreae, 1983; Li et al., 2003).

251       Analysis of CCSEM/EDX data also included calculating the extent of aging across the

252  aerosol size distribution. To obtain this information, nitrogen (N) and sulfur (S) % values for

253  each particle in a cluster of a known particle type were extracted along with the corresponding

254     diameter for each particle. Data was then binned according to diameter size, while N and S %

255     values were averaged for each diameter size. Values that did not exceed 1% were rounded down

256     to 0% as only an exceedance of 1% guarantees the presence of an element.

257           The spatial distribution of elemental components on select particles was also determined

258     using elemental mapping (AZtecLive SmartMapping; Oxford Instruments). Approximately 10

259     elemental maps were collected for dust, sea salt, and internally mixed dust and sea salt. Spectra

260     were collected for select components within elemental maps to obtain more detailed chemistry

261     across an individual particle, which allows for analysis of sea salt and dust components as well

262     as the extent of aging in these components within internally mixed dust and sea salt particles.

263     *2.5 Determination of the Chemical Composition at the Aerosol Surface using Time-of-Flight*

264     *Secondary Ion Mass Spectrometry (TOF-SIMS)*

265           The spatial distribution of major ions across the surface of individual particles was also

266     determined. Aerosol particles were collected onto silicon wafers (Ted Pella, Inc., Prod. # 16008)

267     within the MPS, which were then analyzed with time-of-flight secondary ion mass spectrometry

268     (TOF-SIMS; IONTOF GmbH, Munster, Germany) at PNNL (Li et al., 2023). In addition to

269     providing more detailed chemical information on dust aging, TOF-SIMS supplements the time-

270     intensive method of elemental mapping with SEM/EDX by analyzing multiple particles to

271     explore particle aging, thus supporting the representativeness of elemental mapping results to the

272     total aerosol loading (Hopkins et al., 2008). Further, while EDX is limited to elemental data

273     indicative of aging (e.g., the presence of N and/or S), TOF-SIMS can detect compounds such as

274     nitrate ($NO_3^-$) and sulfate ($HSO_4^-$) ions that more concretely provide evidence of chemical aging.

275           To perform TOF-SIMS analysis, a 25 keV $Bi_3^+$ beam was focused to around a 0.4 μm

276     diameter area on the silicon substrate and scanned over a 100 μm x100 $μm^2$ area to produce an

277    image of 256x256 pixels. The current of the beam was 0.36 pA with 10 kHz pulse frequency,

278    and data collection time was 600 s per set of images. The total ion dose for each sample was

279    under the static limit so that only surface information (<2 nm) was collected for the analyzed

280    particles. Delayed extraction mode was also used during image collection to ensure that both

281    positive and negative ion images could be collected at the exact same location. Ions of interest

282    indicated the presence of sea salt ($Na_2Cl^+$ and $NaCl_2^-$), dust ($Al^+$ and $Ca^+$), and chemical aging

283    ($HSO_4^-$ and $NO_3^-$). Surface contamination from the lab space the samples were handled in (e.g.,

284    butanediol (m/z -89) likely from butanol used in particle counters in the lab space) was observed

285    in the samples, and to remove contamination, a 20 keV argon (Ar) cluster ($Ar_{1500\pm300}^+$) sputtering

286    ion beam was used with a beam current of about 2.0 nA before chemical analysis with the 25

287    keV $Bi_3^+$ beam occurred. Samples underwent Ar sputtering for 50s to remove the top 100 nm of

288    sample.

289    3. **Results**

290    *3.1 Bulk Aerosol Mass Concentrations From Filter Sampling*

291        Figure 1 presents daily dust mass concentrations and bulk soluble ion content along with

292    correlation plots for each ion of interest quantified from our filter samples. Results show a strong

293    correlation between daily dust mass concentrations and nitrate ($NO_3^-$, $R^2 = 0.75$), dust and non-

294    sea salt sulfate (NSS-$SO_4^{2-}$, $R^2 = 0.83$), as well as a weak correlation with oxalate ($R^2 = 0.11$)

295    throughout the entire campaign. The presence of nitrate, non-sea salt sulfate, and oxalate from

296    bulk aerosol analysis suggests that dust is being aged during transport. Similar figures for

297    supermicron (> 1.3 μm)  and submicron (<1.3 μm) analysis can be found in Figures S1 and S2,

298    respectively, in the Supporting Information (SI). Notably, dust mass concentrations were evenly

299    split between the supermicron and submicron size modes. Both supermicron (*SUP*) and

300    submicron (*SUB*) analysis shows similar findings to bulk filter analysis in which a strong

301    correlation exists between dust mass concentrations and nitrate ($R^2_{SUP\,NO3}$ = 0.50; $R^2_{SUB\,NO3}$ =

302    0.59), non-sea salt sulfate ( $R^2_{SUP\,NSS-SO4}$ = 0.80; $R^2_{SUB\,NSS-SO4}$ = 0.49), and oxalate ($R^2_{SUP\,oxalate}$ =

303    0.63; $R^2_{SUB\,oxalate}$ = 0.27). Differences between supermicron and submicron analysis indicate that

304    nitrate is more concentrated in the supermicron aerosol loading ($Avg_{SUP\,NO3}$ = 0.64 $\mu g/m^3$;

305    $Avg_{SUB\,NO3}$ = 0.44 $\mu g/m^3$). However, nitrate has an appreciable submicron mode likely due to

306    transported African smoke. Results also show that $NSS-SO_4^{2-}$ ($Avg_{SUP\,NSS-SO4}$ = 0.04 $\mu g/m^3$;

307    $Avg_{SUB\,NSS-SO4}$ = 0.46 $\mu g/m^3$) and oxalate ($Avg_{SUP\,oxalate}$= 0.01$\mu g/m^3$; $Avg_{SUB\,oxalate}$ = 0.04 $\mu g/m^3$)

308    are more concentrated in the submicron aerosol loading (Quinn et al., 2021; Royer et al., 2023;

309    Savoie et al., 1982). These findings suggest that dust is possibly being aged, with supermicron

310    dust being primarily aged by nitrate and submicron dust being primarily aged by sulfate and

311    oxalate or via cloud processing (Bondy et al., 2017). However, the limitations of this traditional

312    analysis include an oversimplification of aerosol mixing state by assuming nitrate, non-sea salt

313    sulfate, and oxalate are associated only with dust.

314    *3.2 Size-Resolved Aerosol Mixing State from CCSEM/EDX*

315    Using size-resolved chemical data of individual particles from CCSEM/EDX analysis,

316    we assessed the extent of aging across the aerosol size distribution. The role of particle size is

317    important as smaller dust particles have higher surface area-to-volume ratios that have been

318    suggested to increase the propensity for dust aging (Baker & Jickells, 2006). Results from

319    CCSEM/EDX analysis revealed the presence of both marine particles such as sea spray, aged sea

320    spray, organics, and sulfates, as well as continental particle types including dust, internally

321    mixed dust and sea salt, internally mixed dust and smoke from African wildfires, and externally

322    mixed smoke from African wildfires that are described in detail in Royer et al., 2023. Here, we

323 focus on 4 particle types relevant to the understanding of dust aging during the sampling period:

324 dust, sea spray (combined sea spray and aged sea spray), internally mixed dust and sea salt, and

325 internally mixed dust and smoke.

326 Figure 2 presents detailed size-resolved chemical data for the four particle types of

327 interest during periods of dust transport to Barbados, providing insight into the extent of particle

328 aging across the aerosol size distribution. In Figure 2a, particle types are plotted as number

329 fractions of the aerosol loading as a function of aerosol diameter. While dust mass concentrations

330 from our filters for the submicron (<1.3 μm) and supermicron (>1.3 μm) aerosol loading are

331 similar at 14.4 μg/m$^3$ and 12.3 μg/m$^3$, respectively, similar to results found for Asian dust

332 (Zhang et al., 2023), CCSEM analysis reveals that dust only makes up 21% and 4% of the

333 submicron (<1 μm) and supermicron (1-5 μm) aerosol loading by particle number, respectively.

334 We note that part of this discrepancy could be because the CCSEM analysis is restricted to an

335 upper limit of 5 μm in diameter. Figure 2a reveals that internal mixtures of dust with other

336 components such as sea salt and smoke are, in fact, more abundant in the aerosol size distribution

337 compared to dust alone, specifically in the supermicron aerosol loading. Internal mixtures of dust

338 and sea salt comprise 11% of the submicron and 45% of the supermicron aerosol loading, while

339 internal mixtures of dust and smoke comprise 14% of the submicron and 8% of the supermicron

340 aerosol loading. These data reveal a complexity in the aerosol loading overlooked by bulk

341 aerosol analysis, and call into question the assumption that the presence of nitrate, non-sea salt

342 sulfate, and oxalate in bulk samples indicates aging of individual dust particles.

343 Figures 2b, c, d, and e present the average detectable nitrogen (N) content (left axis) and

344 number fraction of N-containing particles (right axis) as a function of particle size for sea salt,

345 internally mixed dust and sea salt, internally mixed dust and smoke, and dust particles,

346  respectively. Values for average N content and particle fractions with detectable N for each

347  particle type are reported in the Supporting Information (SI) tables S1 and S2, respectively.

348  Notably, average N content within individual particles is similar for all 4 particle types, ranging

349  from 2.0±0.5% to 2.6±0.4% N with an average N content of 2.2±0.6%. However, between the 4

350  particle types, there are large variations in the number of particles containing detectable N, which

351  is found in 36±25% of submicron and 76±12% of supermicron dust particles. This corroborates

352  findings from bulk aerosol analysis which shows that nitrate is more concentrated in the

353  supermicron aerosol loading compared to the submicron aerosol loading. However, Figure 2a

354  reveals that dust only comprises 13% of the aerosol loading by number, with a much larger

355  contribution in the submicron aerosol loading. Considering that individual particles containing

356  detectable N on average have a N content of 2.2±0.6%, dust alone cannot explain trends in bulk

357  nitrate. Figure 2c, d, and e all indicate the presence of N in particles aside from dust. Most

358  notably, internally mixed dust and sea salt, which makes up 45% of the supermicron aerosol

359  loading, has detectable N in 75±14% of supermicron particles, potentially explaining the high

360  supermicron nitrate content from bulk aerosol analysis.

361      Figures 2f, g, h, and i present the average detectable sulfur (S) content and number

362  fraction of S-containing particles for the 4 particle types of interest. Values for average S content

363  and particle fractions with detectable S for each particle type are reported in SI tables S3 and S4,

364  respectively. Similarly to Figures 2b, c, d, and e, the S content in individual particles does not

365  vary much across the aerosol size distribution for each particle type, with the average S content

366  for the total aerosol loading ranging from 1.7±0.5% to 2.7±0.5% and averaging 2.4±1.2%.

367  However, the number fractions of particles with detectable S do vary across the aerosol size

368  distribution and between particle types. Only 8±7% of submicron and 14±15% of supermicron

369    dust particles contained detectable S, indicating a large discrepancy between dust particles

370    containing S and the sulfate mass concentrations observed from our filter analysis. For almost all

371    particle types across the aerosol size distribution, with the exception of supermicron internal

372    mixtures of dust and smoke, S content exceeds that of dust. Internal mixtures of dust and sea salt

373    far exceed the S content in dust with $28\pm9\%$ of submicron and $35\pm19\%$ of supermicron

374    internally mixed dust and sea salt particles containing S. This is especially relevant as internal

375    mixtures of dust and sea salt comprise a much larger portion of the supermicron aerosol loading

376    at 45%, compared to dust at 4%. Sea salt particles, which also make up a much larger portion of

377    the particle loading than dust at 55% of the submicron and 44% of the supermicron aerosol

378    loading, also contained larger number fractions of particles with detectable S where $36\pm22\%$ of

379    submicron and $87\pm58\%$ of supermicron sea salt particles had observable S. Observed S in sea

380    salt and internal mixtures of dust and sea salt may explain the observed non-sea salt sulfate mass

381    concentrations detected in the supermicron size range of our filter samples. However, an increase

382    in S in sea salt particles across the size distribution is, in part, likely the result of calcium-sulfate

383    minerals that often form on larger sea salt particles (Ault et al., 2013; Bondy et al., 2018; Choël

384    et al., 2007). Despite the larger mass concentration of non-sea salt sulfate in the submicron size

385    mode of our filters, number fractions of particles containing detectable S were greater in the

386    supermicron size range compared to the submicron size range for all four particle types except

387    internally mixed dust and smoke, which only comprises 14% of the submicron aerosol loading

388    and has an average S content of $2.7\pm1.0\%$ for submicron particles. Instead, high mass

389    concentrations of sulfate observed in submicron IC analysis are likely caused by ammonium

390    sulfate particles observed during the sampling period. Previous studies show sulfate particles are

391    primarily submicron in size and comprise a large fraction of the submicron aerosol loading

392     during both clean marine conditions and African dust transport (Rodriguez et al., 2011), which

393     may contribute high non-sea salt sulfate mass detectable in bulk aerosol analysis but not in S

394     content for the four particle types of interest (Royer et al., 2023).

395        Ternary plots presented in Figure 3 provide insight into the chemical mixing state of

396     detected particles during the EUREC[4]A/ATOMIC campaign. Single particles are represented by

397     individual dots in each ternary plot. The color of each dot indicates the diameter of the particle it

398     represents. The position of each dot within the ternary plot indicates the relative abundance of

399     sulfur (S, left vertex), chlorine (Cl, top vertex), and nitrogen (N, right vertex) within each

400     particle. Sea salt particles displayed in Figure 3a are clustered primarily at the top vertex

401     indicating high Cl content, low S content, and low N content characteristic of freshly emitted sea

402     salt. Particle clustering at the left and right vertices demonstrates aging of sea salt particles as

403     low Cl content and high S and/or N content suggests chloride has been depleted and replaced

404     with nitrate and sulfate during heterogeneous reactions (Ault et al., 2013, 2014; Behnke et al.,

405     1997; Gaston et al., 2011, 2013; Sobanska et al., 2003). Differences in color at each vertex

406     within Figure 3a also indicates that aged sea salt particles are smaller than fresh sea salt particles

407     on average (Laskin et al., 2012).

408        Dust and internally mixed dust and smoke particles are primarily in the submicron size

409     range, as indicated in Figure 2, and cluster at the right vertex indicating the presence of more N

410     compared to S and Cl in these particles, but these particles are sparse in number concentration.

411     Internally mixed dust and sea salt particles cluster primarily along the right axis of the ternary

412     plot, exhibiting various levels of Cl likely from sea salt, low S, and varying N content. Notably,

413     larger particles identified as internally mixed dust and sea salt had elevated chloride compared to

414     S and N while smaller particles had less chloride and elevated S and N. Figure 3 demonstrates

415   that, of the particle types containing dust components, internal mixtures of dust and sea salt are

416   the most abundant in the aerosol loading and had the highest number of aged particles containing

417   detectable N and S. As such, we focus our subsequent analysis of chemical aging on internally

418   mixed dust and sea salt.

419   *3.3 Elemental Mapping and EDX Analysis to Determine Spatial Patterns of Chemical Aging*

420   *Markers on Individual Particles*

421         While analysis by CCSEM/EDX is valuable for determining size-resolved aerosol mixing

422   state, this method does not map the distribution of elements within each particle, which leads to

423   uncertainty regarding the location of the aging components within the particles, particularly for

424   internally mixed particle types. The elemental mapping image depicted in Figure 4a shows the

425   distribution of elements across an entire particle. The presence of distinct areas of dust

426   components such as Si, Al, Ca, Fe, and Mg that are separate from sea salt components such as

427   Na and Cl within a single particle indicates that the particle is a typical internally mixed dust and

428   sea salt particle. Within the image, the distribution of nitrogen and sulfur are depicted as well,

429   and visually appear present only over the sea salt components. Spectra from EDX analysis were

430   extracted from these distinct regions on the particle which reveal that nitrogen and sulfur are

431   indeed either negligible or completely absent on the dust components (S = 0.1%; N = 0%), while

432   they are present in appreciable quantities on the sea salt components (S = 2.9%; N = 2.9%). Also

433   worth noting is the absence of Cl in the sea salt component, which is indicative of sea salt aging

434   also observed in CCSEM/EDX analysis. This particle is representative of internally mixed dust

435   and sea salt particles detected during the sampling period that similarly show only aging on the

436   sea salt components. Additional examples of internally mixed dust and sea salt particle elemental

437   maps and EDX spectra are provided in Figure S3 of the SI. In addition, elemental maps and

438    corresponding EDX spectra for dust, sea salt, smoke, and internally mixed dust and smoke are

439    provided in Figure S4. Similar to the internally mixed dust and sea spray particles, externally

440    mixed dust and the dust component that is internally mixed with smoke show a lack of aging

441    while the smoke components in mixed dust and smoke particles show extensive accumulation of

442    sulfur. These results suggest that even in internal mixtures of dust, only the sea salt (or smoke)

443    components are undergoing aging at least with S while dust shows a lack of chemical aging

444    markers.

445    *3.4 TOF-SIMS Imaging of Chemical Markers of Aerosol Aging*

446         Results from TOF-SIMS analysis corroborate findings from SEM/EDX elemental

447    mapping, indicating that aging of internally mixed dust and sea salt particles occurs primarily on

448    the sea salt components. Figure 5 depicts results from TOF-SIMS imaging in which the color

449    intensity in each image represents the intensity of an ion. The cation images in the top panel

450    indicate the presence of sea salt ($Na_2Cl^+$) and dust ($Al^+$ and $Ca^+$), while the last cation image on

451    the righthand side shows all ions plotted together. The cation image indicates that while the

452    majority of the particles in the image presented are sea salt particles due to the abundance of

453    $Na_2Cl^+$, the co-location of sea salt components with dust components $Al^+$ and $Ca^+$ suggest there

454    is internal mixing of dust and sea salt as well. The anion images in the bottom panel similarly

455    plot individual ions, with the anions indicating the presence of sea salt ($NaCl_2^-$) and chemical

456    markers of aging from sulfate and nitrate ($HSO_4^-$ and $NO_3^-$, respectively) as well as a final image

457    containing all anions plotted together. Once again, the presence of the anion $NaCl_2^-$ suggests that

458    sea salt is abundant and further corroborates the cation images. The presence of $HSO_4^-$ and $NO_3^-$

459    provide insight into the extent of aging on the particles presented in the images which show a

460    strong presence of aging from sulfate through the presence of $HSO_4^-$ but a lack of aging from

461  nitrate through the absence of $NO_3^-$. Most notably, in the image overlaying all anions together,

462  the $NaCl_2^-$ and $HSO_4^-$ are indistinguishable from one another, indicating aging on the sea salt

463  components. Comparing the cation image to the anion image, it is clear that the areas in which

464  dust components are present are not undergoing aging, rather, primarily the sea salt components

465  are being aged. This supports findings from elemental mapping from SEM/EDX analysis which

466  similarly suggest minimal aging of dust components but aging of sea spray components in these

467  internally mixed particles.

468  **4. Conclusions**

469  Traditional methods for studying dust aging often measure dust concentrations (or their

470  proxies) and soluble materials extracted from aerosol filters have historically used correlations

471  between nss-sulfate, oxalate, and nitrate and dust mass concentrations to prove the presence of

472  dust aging. However, these methods have been unable to determine the mixing state of dust and,

473  thus, whether dust (or another aerosol type) is actually undergoing chemical aging (Chen &

474  Siefert, 2004; Li-Jones & Prospero, 1998). The results from this work indicate that while internal

475  mixtures of dust with other particles are common in the lower boundary layer, both internally

476  and externally mixed African dust detected in the western Atlantic are minimally aged during the

477  wintertime. The boreal winter provides the most ideal conditions for African dust chemical aging

478  to occur due to the lower transport altitude creating more time for MBL emissions to interact

479  with long range transported dust. Further, wintertime dust is often co-transported with Sahelian

480  biomass burning and industrial emissions contributing high concentrations of NOx and $SO_2$ that

481  are co-transported with dust, allowing for interaction of dust with gases that can induce chemical

482  aging over several days during transatlantic transport (Hickman et al., 2021). The lack of aging

483  on internal mixtures of dust and smoke indicate rapid conversion of $NO_x$ and $SO_2$ to nitrate and

484  sulfate on smoke, which is corroborated by the presence of potassium sulfate salts observed on

485  smoke particles from EUREC[4]A/ATOMIC and a lack of these compounds on dust (Royer et al.,

486  2023). The lack of dust aging indicators observed during the winter may indicate a lack of aging

487  throughout the year for long range transported African dust. This is apparent from size-resolved

488  CCSEM/EDX data which indicate a lack of aging on dust particles by sulfate and nitrate, and

489  from elemental mapping and TOF-SIMS imaging which show that chemical aging is favored on

490  the sea spray and smoke components of internally mixed dust particles. Our findings of aged sea

491  spray, with losses of chloride, on internally mixed dust and sea spray particles could also indicate

492  an increase in the heterogeneous displacement of chloride from these internally mixed particles

493  compared to sea spray alone (van Herpen et al., 2023).

494  It is likely that dust is being aged in the eastern Atlantic, but is removed during long

495  range transport to the western Atlantic based on previous studies (Abdelkader et al., 2017). The

496  lower altitude for dust transport during the wintertime would also provide ample opportunity for

497  dust aging in the eastern Atlantic which could lead to the rapid aging of dust particles before

498  long range transport (Chiapello et al., 1995; Kandler et al., 2011; Ullerstam et al., 2002). The

499  addition of high levels of pollutants from North African industrial emissions and the Sahelian

500  fires could also exacerbate aging in the eastern Atlantic (Andreae et al., 2000; Rodriguez et al.,

501  2011). Aged dust particles are much more efficiently removed by both wet and dry deposition as

502  well as cloud droplet activation as a result of increased water uptake properties enhancing their

503  size and reactivity (Abdelkader et al., 2017; Gaston, 2020; Metzger et al., 2006). It is possible

504  that the rapid aging of dust particles in the eastern Atlantic upon dust emission increases the

505  water uptake properties of the dust, leading to rapid removal of dust particles before long range

506  transport can carry dust particles to the western Atlantic. This potentially explains the minimal

507  aging of dust particles in the western Atlantic, as any aged dust is likely removed before arriving

508  over Barbados.

509      Based on the high abundance of internally mixed dust and sea salt particles in the aerosol

510  loading, it is likely that unaged dust transported across the Atlantic becomes associated with

511  aged sea spray as dust is being detrained from the SAL into the MBL as suggested in previous

512  studies (Abdelkader et al., 2017). This would result in altitudinal gradients in dust mixing state

513  important for dust radiative impacts. Though dust components in the lower boundary layer are

514  rarely aged, internal mixtures of dust with other components such as sea salt and smoke are

515  common. The high degree of aging on these internally mixed components suggest internal dust

516  mixtures are more hygroscopic and, thus, are potentially efficient as cloud condensation nuclei.

517      The lack of aging on dust components has implications for nutrient availability in mineral

518  dust aerosols transported to the tropical Atlantic as well. Ecosystems in the tropical Atlantic such

519  as the open Atlantic Ocean and the Amazon rainforest rely on external inputs of nutrients such as

520  iron and phosphorus (Fe and P). Chemical aging is particularly important to provide bioavailable

521  sources of nutrients to marine ecosystems, as deposition of particles out of the euphotic zone

522  competes with nutrient release into seawater (Gaston, 2020). The lack of chemical aging on

523  mineral dust observed in this study suggests that the chemical aging of dust plays a limited role

524  in observed increases in nutrient solubility during transatlantic transport, consistent with findings

525  for Asian dust (Chen et al, 2024).

526      In this work, we utilized methods that target aerosol mixing state to determine the extent

527  of aging in long range transported African dust particles to the western Atlantic during the

528  wintertime. The disparity between bulk methods, which suggest dust aging is extensive, and

529  methods that characterize the aerosol mixing state, which reveal a distinct lack of aging for dust

530     components, reveals the importance of utilizing single-particle methods to understand dust aging

531     (Fitzgerald et al., 2015; Kandler et al., 2011). We also provide much-needed insight into the

532     question of dust aging in the western Atlantic, revealing limited aging for dust particles in the

533     wintertime that should be considered in global and regional models.

534     **Data Availability**

535     Dust and soluble ion mass concentration data and number counts of particle types detected by

536     CCSEM/EDX are publicly available in the University of Miami data repository

537     https://doi.org/10.17604/xgaz-cb40.

538     **Author Contribution:**

539     Conceptualization of this work was performed by HMR, APA, and CJG. Collection of

540     samples was conducted by HMR and EB, while analysis was done by HMR, MS, HE, NNL, ZC,

541     and ZZ. Development of methods used in this work was done by HMR, ZC, SC, APA, and CJG.

542     Instrumentation used to conduct this work was provided by CJG, APA, SC, and ZZ.

543     Validation of data products was performed by HMR, ZC, APA, and CJG. Computer code used

544     for data analysis was provided by APA. Data visualization was performed by HMR, APA,

545     and CJG. Supervision and project administration duties were conducted by CJG. CJG is

546     responsible for funding acquisition. HMR wrote the original draft for publication, and all co-

547     authors reviewed and edited this work.

548
549
550     **Competing Interests:** The authors declare that they have no conflict of interest.
551

552     **Acknowledgements**

553     C.J.G. acknowledges an NSF CAREER award (1944958). A portion of this research was

554     performed on project awards (10.46936/lser.proj.2019.50816/60000110 and

555    10.46936/lser.proj.2021.51900/60000361) from the Environmental Molecular Sciences

556    Laboratory, a DOE Office of Science User Facility sponsored by the Biological and

557    Environmental Research program under Contract No. DE-AC05-76RL01830.

558
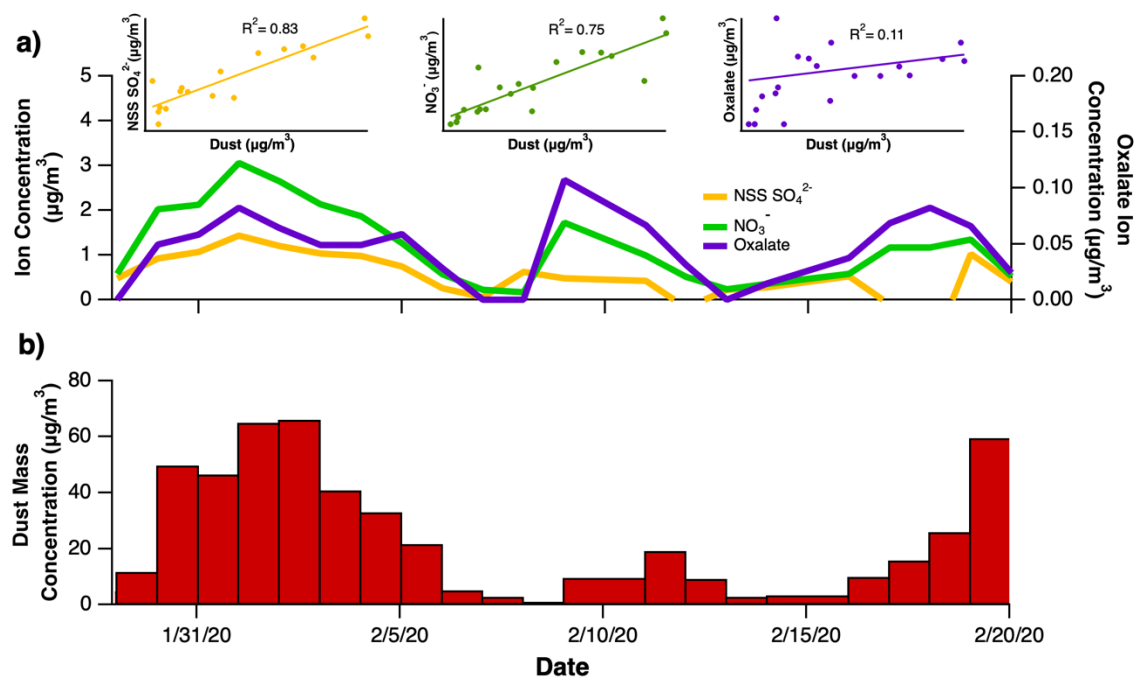
559    Figure 1 – a) Daily bulk soluble ion content for nitrate (left axis; green line), non-sea salt sulfate

560    (left axis; yellow line), and oxalate (right axis; purple line) with correlation plots for each ion as

561    a function of dust mass concentrations and b) daily bulk dust mass concentrations determined for

562    the entire sampling period. Correlation plots include all data, including data from samples with

563    undetectable ions, but trendlines only consider data with detectable dust and ions.

564

565
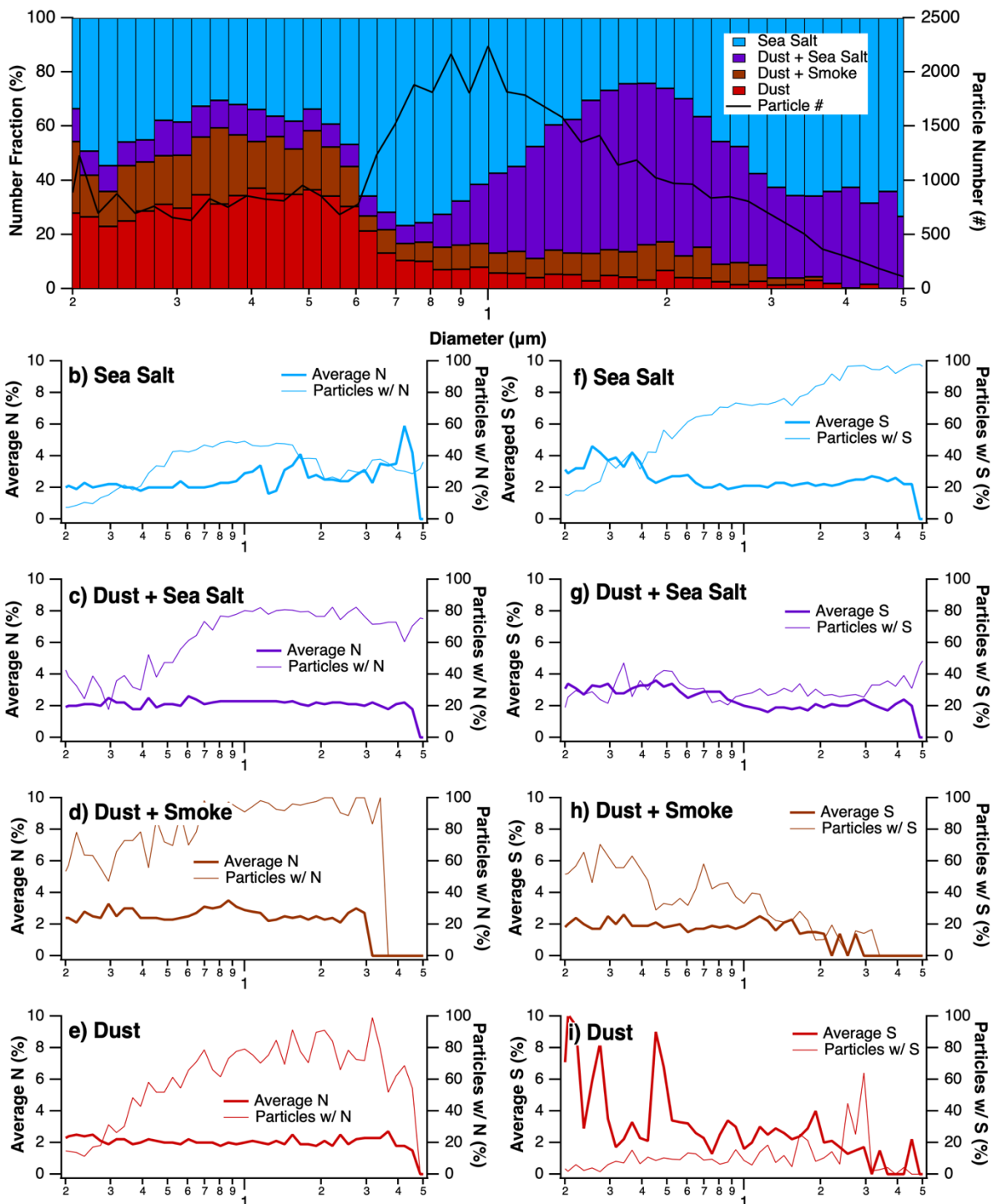
Figure 2 – Size-resolved chemistry plots summarized by a) a total size-resolved chemistry plot in

which the particle number loading is normalized to the sum of sea salt particles (blue), internally

mixed dust and sea salt particles (purple), internally mixed dust and smoke particles (brown), and

569    dust particles (red) for each size bin and presented as a fraction of the particle number loading in

570    each size bin (left axis) along with the total sum of the number of particles of interest for each

571    size bin (right axis: black line). Plots depicting the average nitrogen (N) or sulfur (S) content in

572    individual particles (left axis; thick line) as well as the number fraction of particles in each size

573    bin containing nitrogen or sulfur (right axis; thin line) are provided for b) nitrogen in sea salt

574    particles, c) nitrogen in internally mixed dust and sea salt particles, d) nitrogen in internally

575    mixed dust and smoke particles, e) nitrogen in dust particles, f) sulfur in sea salt particles, g)

576    sulfur in internally mixed dust and sea salt particles, h) sulfur in internally mixed dust and smoke

577    particles, and i) sulfur in dust particles.
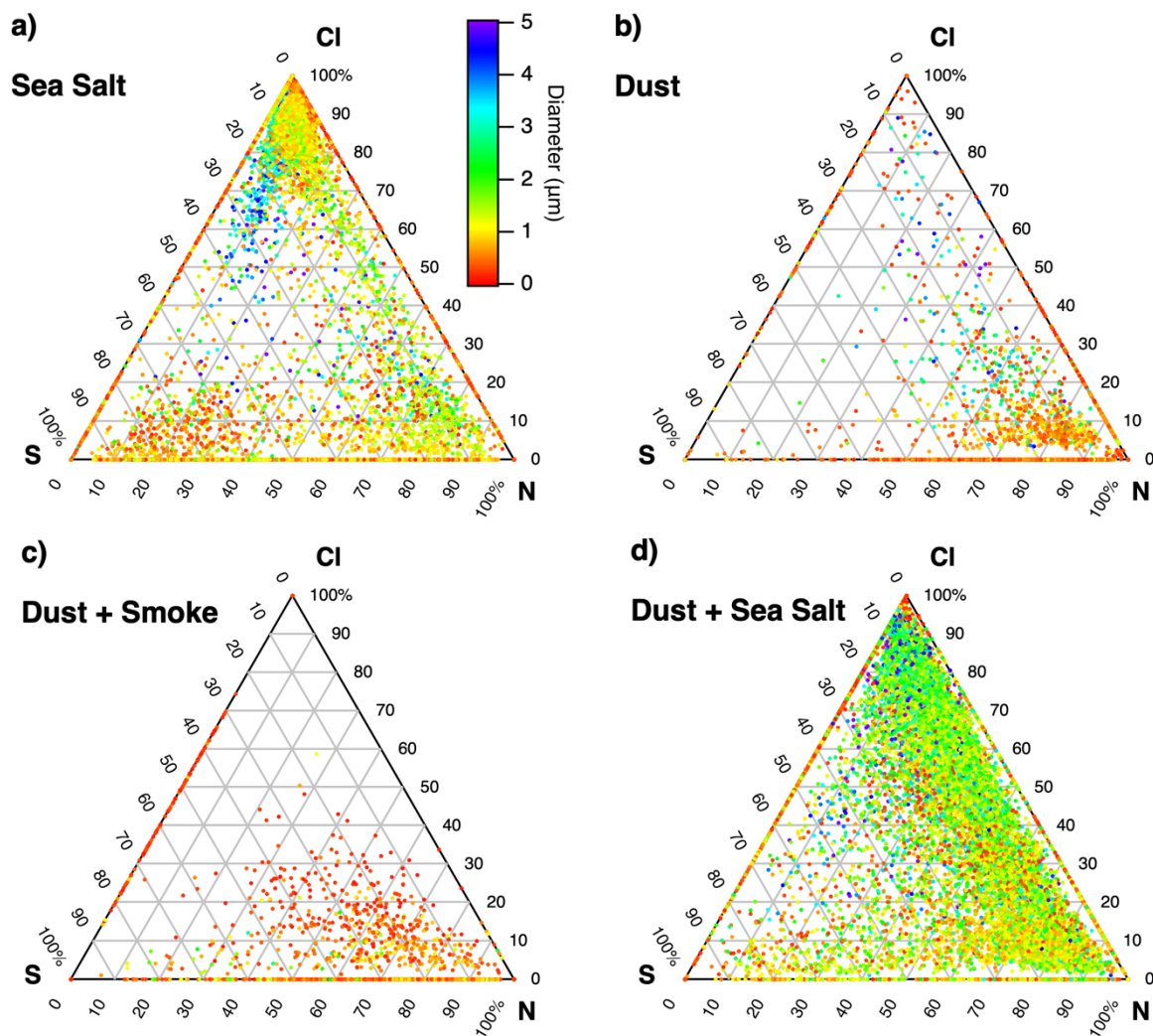
578

579 Figure 3 – Ternary plots presenting the normalized percentage of sulfur (S) (left axis), chlorine

580 (Cl), (right axis), and nitrogen (N) (bottom axis) present in dust (6,426 particles), internally

581 mixed dust + smoke (1,588 particles), internally mixed dust + sea salt (18,210 particles), and sea

582 salt (22,354 particles). Color scaling denotes particle diameter.
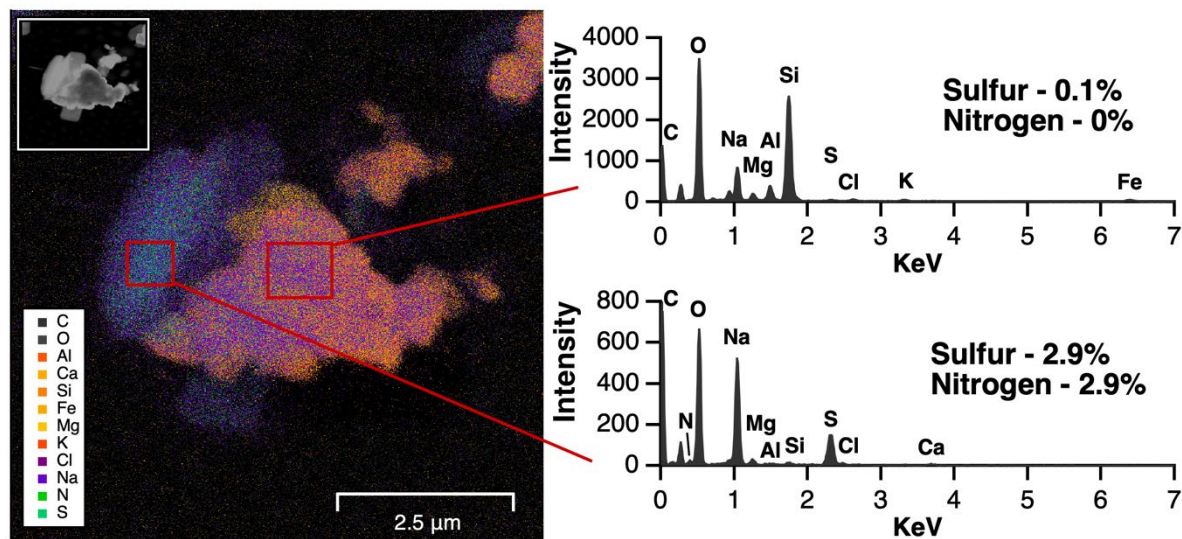
583

584 Figure 4 – Elemental mapping image from SEM/EDX analysis for an internally mixed dust and

585 sea salt particle collected at Ragged Point on 2/9/2020 on stage 2 of the MPS. Top left plot

586 depicts the SEM image. The legend explains the color associated with each element plotted in

587 the elemental map with warm colors denoting dust components, cool colors denoting sea spray

588 components and green colors denoting aging markers. Red squares on the elemental map indicate

589 where EDX spectra were extracted for the dust component, which is shown in the top right plot,

590 and the sea salt component, shown in the bottom right plot, of the particle. Sulfur and nitrogen

591 values represent calculated EDX intensity present on dust and sea spray components of the

592 particle.

593
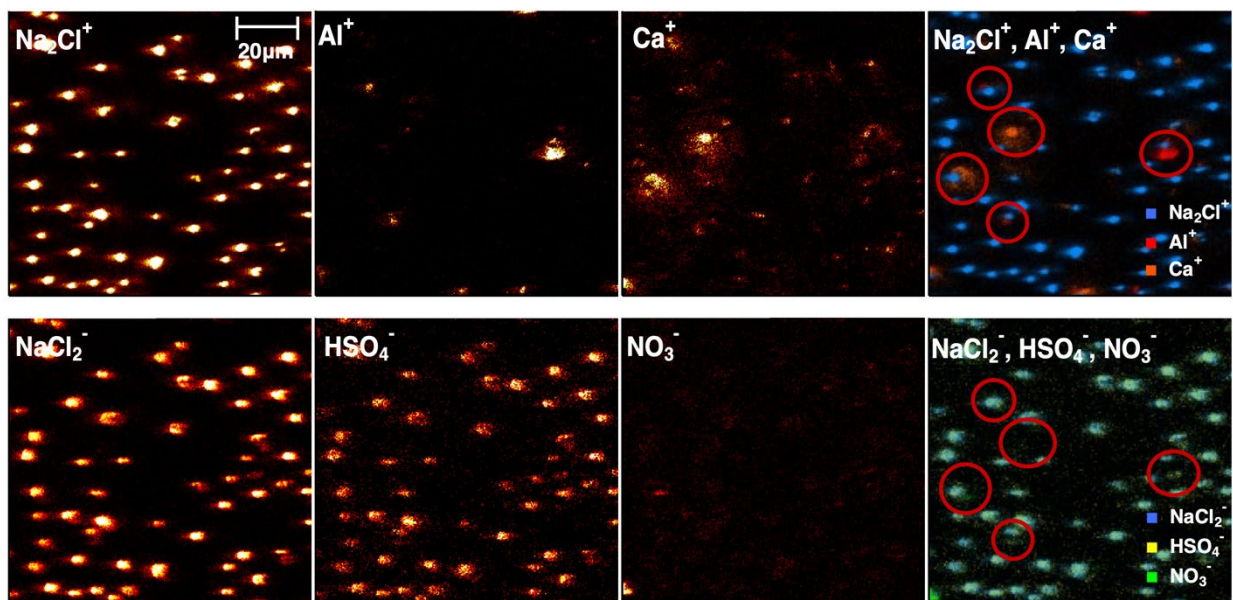
594     Figure 5 – Image plots from TOF-SIMS analysis of a sample collected on 2/18/2020 from stage

595     1 of the MPS. Red circles mark the location of dust components of the particles. The top panel

596     shows images of cations indicative of sea salt ($Na_2Cl^+$), dust ($Al^+$ and $Ca^+$), and a combined plot

597     showing all three markers. The bottom panel shows anions indicative of sea salt ($NaCl_2^-$),

598     chemical aging markers (sulfate ($HSO_4^-$), nitrate ($NO_3^-$)) and a combined plot showing all three

599     markers.

600
601
602
603
604
605
606
607
608
609
610
611
612
613
614

**References**

Abdelkader, M., Metzger, S., Mamouri, R. E., Astitha, M., Barrie, L., Levin, Z., & Lelieveld, J. (2015). Dust–air pollution dynamics over the eastern Mediterranean. *Atmospheric Chemistry and Physics*, *15*(16), 9173–9189. https://doi.org/10.5194/acp-15-9173-2015

Abdelkader, M., Metzger, S., Steil, B., Klingmüller, K., Tost, H., Pozzer, A., Stenchikov, G., Barrie, L., & Lelieveld, J. (2017). Sensitivity of transatlantic dust transport to chemical aging and related atmospheric processes. *Atmospheric Chemistry and Physics*, *17*(6), 3799–3821. https://doi.org/10.5194/acp-17-3799-2017

Albrecht, B. A. (1989). Aerosols, cloud microphysics, and fractional cloudiness. *Science*, *245*(4923), 1227–1230. https://doi.org/10.1126/science.245.4923.1227

Andreae, M O, Elbert, W., Gabriel, R., Johnson, D. W., Osborne, S., & Wood, R. (2000). Soluble ion chemistry of the atmospheric aerosol and SO2 concentrations over the eastern North Atlantic during ACE-2. *Tellus B: Chemical and Physical Meteorology*. https://doi.org/10.3402/tellusb.v52i4.17087

Andreae, Meinrat O. (1983). Soot Carbon and Excess Fine Potassium: Long-Range Transport of Combustion-Derived Aerosols. *Science*, *220*(4602), 1148–1151. https://doi.org/10.1126/science.220.4602.1148

Andreae, Meinrat O, Charlson, R. J., Bruynseels, F., Storms, H., Grieken, R. Van, & Maenhaut, W. (1986). Internal Mixture of Sea Salt, Silicates, and Excess Sulfate in Marine Aerosols. *Science*, *232*(4758), 1620–1623. https://doi.org/10.1126/science.232.4758.1620

Archibald, A. T., Witham, C. S., Ashfold, M. J., Manning, A. J., O'Doherty, S., Greally, B. R., Young, D., & Shallcross, D. E. (2015). Long-term high frequency measurements of ethane, benzene and methyl chloride at Ragged Point, Barbados: Identification of long-range transport events. *Elementa: Science of the Anthropocene*, *3*. https://doi.org/10.12952/journal.elementa.000068

Archuleta, C. M., DeMott, P. J., & Kreidenweis, S. M. (2005). Ice nucleation by surrogates for atmospheric mineral dust and mineral dust/sulfate particles at cirrus temperatures. *Atmospheric Chemistry and Physics*, *5*(10), 2617–2634. https://doi.org/10.5194/acp-5-2617-2005

Ault, A. P., Peters, T. M., Sawvel, E. J., Casuccio, G. S., Willis, R. D., Norris, G. A., & Grassian, V. H. (2012). Single-Particle SEM-EDX Analysis of Iron-Containing Coarse Particulate Matter in an Urban Environment: Sources and Distribution of Iron within Cleveland, Ohio. *Environmental Science & Technology*, *46*(8), 4331–4339. https://doi.org/10.1021/es204006k

Ault, A. P., Moffet, R. C., Baltrusaitis, J., Collins, D. B., Ruppel, M. J., Cuadra-Rodriguez, L. A., Zhao, D., Guasco, T. L., Ebben, C. J., Geiger, F. M., Bertram, T. H., Prather, K. A., & Grassian, V. H. (2013). Size-Dependent Changes in Sea Spray Aerosol Composition and Properties with Different Seawater Conditions. *Environmental Science & Technology*, *47*(11), 5603–5612. https://doi.org/10.1021/es400416g

Ault, A. P., Guasco, T. L., Baltrusaitis, J., Ryder, O. S., Trueblood, J. V, Collins, D. B., Ruppel, M. J., Cuadra-Rodriguez, L. A., Prather, K. A., & Grassian, V. H. (2014). Heterogeneous Reactivity of Nitric Acid with Nascent Sea Spray Aerosol: Large Differences Observed between and within Individual Particles. *The Journal of Physical Chemistry Letters*, *5*(15), 2493–2500. https://doi.org/10.1021/jz5008802

Baker, A. R., & Jickells, T. D. (2006). Mineral particle size as a control on aerosol iron

solubility. *Geophysical Research Letters*, *33*(17), 1–4.
https://doi.org/10.1029/2006GL026557

Balkanski, Y., Schulz, M., Claquin, T., & Guibert, S. (2007). Reevaluation of Mineral aerosol radiative forcings suggests a better agreement with satellite and AERONET data. *Atmospheric Chemistry and Physics*, *7*(1), 81–95. https://doi.org/10.5194/acp-7-81-2007

Barkley, A. E., Prospero, J. M., Mahowald, N., Hamilton, D. S., Popendorf, K. J., Oehlert, A. M., Pourmand, A., Gatineau, A., Panechou-Pulcherie, K., Blackwelder, P., & Gaston, C. J. (2019). African biomass burning is a substantial source of phosphorus deposition to the Amazon, Tropical Atlantic Ocean, and Southern Ocean. *Proceedings of the National Academy of Sciences*, *116*(33), 16216 LP – 16221. https://doi.org/10.1073/pnas.1906091116

Bauer, S. E., Mishchenko, M. I., Lacis, A. A., Zhang, S., Perlwitz, J., & Metzger, S. M. (2007). Do sulfate and nitrate coatings on mineral dust have important effects on radiative properties and climate modeling? *Journal of Geophysical Research: Atmospheres*, *112*(D6). https://doi.org/https://doi.org/10.1029/2005JD006977

Behnke, W., George, C., Scheer, V., & Zetzsch, C. (1997). Production and decay of $ClNO_2$ from the reaction of gaseous $N_2O_5$ with NaCl solution: Bulk and aerosol experiments. *Journal of Geophysical Research Atmospheres*, *102*(3), 3795–3804. https://doi.org/10.1029/96jd03057

Bondy, A L, Bonanno, D., Moffet, R. C., Wang, B., Laskin, A., & Ault, A. P. (2018). The diverse chemical mixing state of aerosol particles in the southeastern United States. *Atmospheric Chemistry and Physics*, *18*(16), 12595–12612. https://doi.org/10.5194/acp-18-12595-2018

Bondy, Amy L, Wang, B., Laskin, A., Craig, R. L., Nhliziyo, M. V, Bertman, S. B., Pratt, K. A., Shepson, P. B., & Ault, A. P. (2017). Inland Sea Spray Aerosol Transport and Incomplete Chloride Depletion: Varying Degrees of Reactive Processing Observed during SOAS. *Environmental Science & Technology*, *51*(17), 9533–9542. https://doi.org/10.1021/acs.est.7b02085

Carlson, T. N., & Prospero, J. M. (1972). The Large-Scale Movement of Saharan Air Outbreaks over the Northern Equatorial Atlantic. *Journal of Applied Meteorology and Climatology*, *11*(2), 283–297. https://doi.org/10.1175/1520-0450(1972)011<0283:TLSMOS>2.0.CO;2

Chen, Y., & Siefert, R. L. (2004). Seasonal and spatial distributions and dry deposition fluxes of atmospheric total and labile iron over the tropical and subtropical North Atlantic Ocean. *Journal of Geophysical Research: Atmospheres*, *109*(D9). https://doi.org/https://doi.org/10.1029/2003JD003958

Chen, Y.Z., Wang, Z.Y., Fang, Z.Y., Huang, C.P., Xu, H., Zhang, H.H., Zhang, T.Y., Wang, F., Luo, L., Shi, G.L., Wang, X.M., & Tang, M.J. (2024) Dominant contribution of non-dust primary emissions and secondary processes to dissolved aerosol iron. *Environmental Science & Technology*, *58*, 17355-17363.

Chiapello, I., Bergametti, G., Gomes, L., Chatenet, B., Dulac, F., Pimenta, J., & Suares, E. S. (1995). An additional low layer transport of Sahelian and Saharan dust over the north-eastern Tropical Atlantic. *Geophysical Research Letters*, *22*(23), 3191–3194. https://doi.org/https://doi.org/10.1029/95GL03313

Choël, M., Deboudt, K., Flament, P., Aimoz, L., & Mériaux, X. (2007). Single-particle analysis of atmospheric aerosols at Cape Gris-Nez, English Channel: Influence of steel works on iron apportionment. *Atmospheric Environment*, *41*(13), 2820–2830. https://doi.org/https://doi.org/10.1016/j.atmosenv.2006.11.038

Cziczo, D. J., Murphy, D. M., Hudson, P. K., & Thomson, D. S. (2004). Single particle

measurements of the chemical composition of cirrus ice residue during CRYSTAL-FACE. *Journal of Geophysical Research: Atmospheres*, *109*(D4). https://doi.org/https://doi.org/10.1029/2003JD004032

DeMott, P. J., Sassen, K., Poellot, M. R., Baumgardner, D., Rogers, D. C., Brooks, S. D., Prenni, A. J., & Kreidenweis, S. M. (2003). African dust aerosols as atmospheric ice nuclei. *Geophysical Research Letters*, *30*(14). https://doi.org/https://doi.org/10.1029/2003GL017410

Denjean, C., Caquineau, S., Desboeufs, K., Laurent, B., Maille, M., Quiñones Rosado, M., Vallejo, P., Mayol-Bracero, O. L., & Formenti, P. (2015). Long-range transport across the Atlantic in summertime does not enhance the hygroscopicity of African mineral dust. *Geophysical Research Letters*, *42*(18), 7835–7843. https://doi.org/https://doi.org/10.1002/2015GL065693

Desboeufs, K., Formenti, P., Torres-Sánchez, R., Schepanski, K., Chaboureau, J.-P., Andersen, H., Cermak, J., Feuerstein, S., Laurent, B., Klopper, D., Namwoonde, A., Cazaunau, M., Chevaillier, S., Feron, A., Mirande-Bret, C., Triquet, S., & Piketh, S. J. (2024). Fractional solubility of iron in mineral dust aerosols over coastal Namibia: a link to marine biogenic emissions? *Atmospheric Chemistry and Physics*, *24*(2), 1525–1541. https://doi.org/10.5194/acp-24-1525-2024

Elliott, H. E., Popendorf, K. J., Blades, E., Royer, H. M., Pollier, C. G. L., Oehlert, A. M., Kukkadapu, R., Ault, A., & Gaston, C. J. (2024). Godzilla mineral dust and La Soufrière volcanic ash fallout immediately stimulate marine microbial phosphate uptake, *10*. https://doi.org/https://doi.org/10.3389/fmars.2023.1308689

Fitzgerald, E., Ault, A. P., Zauscher, M. D., Mayol-Bracero, O. L., & Prather, K. A. (2015). Comparison of the mixing state of long-range transported Asian and African mineral dust. *Atmospheric Environment*, *115*, 19–25. https://doi.org/https://doi.org/10.1016/j.atmosenv.2015.04.031

Gaston, C. J. (2020). Re-examining Dust Chemical Aging and Its Impacts on Earth's Climate. *Accounts of Chemical Research*, *53*(5), 1005–1013. https://doi.org/10.1021/acs.accounts.0c00102

Gaston, C. J., Pratt, K. A., Qin, X., & Prather, K. A. (2010). Real-time detection and mixing state of methanesulfonate in single particles at an inland urban location during a phytoplankton bloom. *Environmental Science and Technology*, *44*(5), 1566–1572. https://doi.org/10.1021/es902069d

Gaston, C. J., Furutani, H., Guazzotti, S. A., Coffee, K. R., Bates, T. S., Quinn, P. K., Aluwihare, L. I., Mitchell, B. G., & Prather, K. A. (2011). Unique ocean-derived particles serve as a proxy for changes in ocean chemistry. *Journal of Geophysical Research Atmospheres*, *116*(18), 1–13. https://doi.org/10.1029/2010JD015289

Gaston, C. J., Quinn, P. K., Bates, T. S., Gilman, J. B., Bon, D. M., Kuster, W. C., & Prather, K. A. (2013). The impact of shipping, agricultural, and urban emissions on single particle chemistry observed aboard the R/V Atlantis during CalNex. *Journal of Geophysical Research Atmospheres*, *118*(10), 5003–5017. https://doi.org/10.1002/jgrd.50427

Gaston, C.J., Prospero, J.M., Foley, K., Pye, H.O.T., Custals, L., Blades, E., Sealy, P., & Christie, J.A. (2024) Diverging trends in aerosol sulfate and nitrate measured in the remote North Atlantic on Barbados are attricuted to clean air policies, African smoke, and anthropogenic emissions. *Atmospheric Chemistry & Physics*, *24*(13), 8049-8066.

Gibson, E. R., Gierlus, K. M., Hudson, P. K., & Grassian, V. H. (2007). Generation of Internally

Mixed Insoluble and Soluble Aerosol Particles to Investigate the Impact of Atmospheric Aging and Heterogeneous Processing on the CCN Activity of Mineral Dust Aerosol. *Aerosol Science and Technology*, *41*(10), 914–924. https://doi.org/10.1080/02786820701557222

Gierlus, K. M., Laskina, O., Abernathy, T. L., & Grassian, V. H. (2012). Laboratory study of the effect of oxalic acid on the cloud condensation nuclei activity of mineral dust aerosol. *Atmospheric Environment*, *46*, 125–130. https://doi.org/https://doi.org/10.1016/j.atmosenv.2011.10.027

Gutleben, M., Groß, S., Heske, C., & Wirth, M. (2022). Wintertime Saharan dust transport towards the Caribbean: an airborne lidar case study during EUREC[4]A. *Atmospheric Chemistry and Physics*, *22*(11), 7319–7330. https://doi.org/10.5194/acp-22-7319-2022

Han, X., Zhang, M., Han, Z., Xin, J., & Liu, X. (2011). Simulation of aerosol direct radiative forcing with RAMS-CMAQ in East Asia. *Atmospheric Environment*, *45*(36), 6576–6592. https://doi.org/https://doi.org/10.1016/j.atmosenv.2011.08.006

Hand, V. L., Capes, G., Vaughan, D. J., Formenti, P., Haywood, J. M., & Coe, H. (2010). Evidence of internal mixing of African dust and biomass burning particles by individual particle analysis using electron beam techniques. *Journal of Geophysical Research: Atmospheres*, *115*(D13). https://doi.org/https://doi.org/10.1029/2009JD012938

Haywood, J., Francis, P., Osborne, S., Glew, M., Loeb, N., Highwood, E., Tanré, D., Myhre, G., Formenti, P., & Hirst, E. (2003). Radiative properties and direct radiative effect of Saharan dust measured by the C-130 aircraft during SHADE: 1. Solar spectrum. *Journal of Geophysical Research: Atmospheres*, *108*(D18). https://doi.org/https://doi.org/10.1029/2002JD002687

Hickman, J. E., Andela, N., Tsigaridis, K., Galy-Lacaux, C., Ossohou, M., & Bauer, S. E. (2021). Reductions in $NO_2$ burden over north equatorial Africa from decline in biomass burning in spite of growing fossil fuel use, 2005 to 2017. *Proceedings of the National Academy of Sciences*, *118*(7), e2002579118. https://doi.org/10.1073/pnas.2002579118

Hopkins, R. J., Desyaterik, Y., Tivanski, A. V, Zaveri, R. A., Berkowitz, C. M., Tyliszczak, T., Gilles, M. K., & Laskin, A. (2008). Chemical speciation of sulfur in marine cloud droplets and particles: Analysis of individual particles from the marine boundary layer over the California current. *Journal of Geophysical Research: Atmospheres*, *113*(D4). https://doi.org/https://doi.org/10.1029/2007JD008954

Jickells, T. D., An, Z. S., Andersen, K. K., Baker, A. R., Bergametti, G., Brooks, N., Cao, J. J., Boyd, P. W., Duce, R. A., Hunter, K. A., Kawahata, H., Kubilay, N., laRoche, J., Liss, P. S., Mahowald, N., Prospero, J. M., Ridgwell, A. J., Tegen, I., & Torres, R. (2005). Global Iron Connections Between Desert Dust, Ocean Biogeochemistry, and Climate. *Science*, *308*(5718), 67–71. https://doi.org/10.1126/science.1105959

Kandler, K., Lieke, K., Benker, N., Emmel, C., Küpper, M., Müller-Ebert, D., Ebert, M., Scheuvens, D., Schladitz, A., Schütz, L., & Weinbruch, S. (2011). Electron microscopy of particles collected at Praia, Cape Verde, during the Saharan Mineral Dust Experiment: particle chemistry, shape, mixing state and complex refractive index. *Tellus B: Chemical and Physical Meteorology*, *63*(4), 475–496. https://doi.org/10.1111/j.1600-0889.2011.00550.x

Kandler, K., Schneiders, K., Ebert, M., Hartmann, M., Weinbruch, S., Prass, M., & Pöhlker, C. (2018). Composition and mixing state of atmospheric aerosols determined by electron microscopy: method development and application to aged Saharan dust deposition in the

799 Caribbean boundary layer. *Atmos. Chem. Phys.*, *18*(18), 13429–13455.
800 https://doi.org/10.5194/acp-18-13429-2018

801 Kelly, J. T., Chuang, C. C., & Wexler, A. S. (2007). Influence of dust composition on cloud
802 droplet formation. *Atmospheric Environment*, *41*(14), 2904–2916.
803 https://doi.org/10.1016/j.atmosenv.2006.12.008

804 Koehler, K. A., Kreidenweis, S. M., DeMott, P. J., Petters, M. D., Prenni, A. J., & Carrico, C. M.
805 (2009). Hygroscopicity and cloud droplet activation of mineral dust aerosol. *Geophysical*
806 *Research Letters*, *36*(8). https://doi.org/https://doi.org/10.1029/2009GL037348

807 Krueger, B. J., Grassian, V. H., Laskin, A., & Cowin, J. P. (2003). The transformation of solid
808 atmospheric particles into liquid droplets through heterogeneous chemistry: Laboratory
809 insights into the processing of calcium containing mineral dust aerosol in the troposphere.
810 *Geophysical Research Letters*, *30*(3). https://doi.org/https://doi.org/10.1029/2002GL016563

811 Krueger, B. J., Grassian, V. H., Cowin, J. P., & Laskin, A. (2004). Heterogeneous chemistry of
812 individual mineral dust particles from different dust source regions: The importance of
813 particle mineralogy. *Atmospheric Environment*, *38*(36), 6253–6261.
814 https://doi.org/10.1016/j.atmosenv.2004.07.010

815 Lance, S., Raatikainen, T., Onasch, T. B., Worsnop, D. R., Yu, X.-Y., Alexander, M. L.,
816 Stolzenburg, M. R., McMurry, P. H., Smith, J. N., & Nenes, A. (2013). Aerosol mixing
817 state, hygroscopic growth and cloud activation efficiency during MIRAGE 2006.
818 *Atmospheric Chemistry and Physics*, *13*(9), 5049–5062. https://doi.org/10.5194/acp-13-
819 5049-2013

820 Laskin, A, Wietsma, T. W., Krueger, B. J., & Grassian, V. H. (2005). Heterogeneous chemistry
821 of individual mineral dust particles with nitric acid: A combined CCSEM/EDX, ESEM, and
822 ICP-MS study. *Journal of Geophysical Research: Atmospheres*, *110*(D10).
823 https://doi.org/https://doi.org/10.1029/2004JD005206

824 Laskin, Alexander, Moffet, R. C., Gilles, M. K., Fast, J. D., Zaveri, R. A., Wang, B., Nigge, P.,
825 & Shutthanandan, J. (2012). Tropospheric chemistry of internally mixed sea salt and
826 organic particles: Surprising reactivity of NaCl with weak organic acids. *Journal of*
827 *Geophysical Research: Atmospheres*, *117*(D15).
828 https://doi.org/https://doi.org/10.1029/2012JD017743

829 Levin, Z, Teller, A., Ganor, E., & Yin, Y. (2005). On the interactions of mineral dust, sea-salt
830 particles, and clouds: A measurement and modeling study from the Mediterranean Israeli
831 Dust Experiment campaign. *Journal of Geophysical Research: Atmospheres*, *110*(D20).
832 https://doi.org/https://doi.org/10.1029/2005JD005810

833 Levin, Zev, Ganor, E., & Gladstein, V. (1996). The Effects of Desert Particles Coated with
834 Sulfate on Rain Formation in the Eastern Mediterranean. *Journal of Applied Meteorology*
835 *and Climatology*, *35*(9), 1511–1523. https://doi.org/https://doi.org/10.1175/1520-
836 0450(1996)035<1511:TEODPC>2.0.CO;2

837 Li-Jones, X., & Prospero, J. M. (1998). Variations in the size distribution of non-sea-salt sulfate
838 aerosol in the marine boundary layer at Barbados: Impact of African dust. *Journal of*
839 *Geophysical Research: Atmospheres*, *103*(D13), 16073–16084.
840 https://doi.org/https://doi.org/10.1029/98JD00883

841 Li, J., Pósfai, M., Hobbs, P. V, & Buseck, P. R. (2003). Individual aerosol particles from
842 biomass burning in southern Africa: 2, Compositions and aging of inorganic particles.
843 *Journal of Geophysical Research: Atmospheres*, *108*(D13).
844 https://doi.org/https://doi.org/10.1029/2002JD002310

845  Li, W., Shao, L., Shi, Z., Chen, J., Yang, L., Yuan, Q., Yan, C., Zhang, X., Wang, Y., Sun, J.,
846      Zhang, Y., Shen, X., Wang, Z., & Wang, W. (2014). Mixing state and hygroscopicity of
847      dust and haze particles before leaving Asian continent. *Journal of Geophysical Research:*
848      *Atmospheres*, *119*(2), 1044–1059. https://doi.org/https://doi.org/10.1002/2013JD021003
849  Li, Y., Zhou, Y., Guo, W., Zhang, X., Huang, Y., He, E., Li, R., Yan, B., Wang, H., Mei, F., Liu,
850      M., & Zhu, Z. (2023). Molecular Imaging Reveals Two Distinct Mixing States of PM2.5
851      Particles Sampled in a Typical Beijing Winter Pollution Case. *Environmental Science &*
852      *Technology*, *57*(15), 6273–6283. https://doi.org/10.1021/acs.est.2c08694
853  Ma, C.-J., Tohno, S., Kasahara, M., & Hayakawa, S. (2004). Properties of the size-resolved and
854      individual cloud droplets collected in western Japan during the Asian dust storm event.
855      *Atmospheric Environment*, *38*(27), 4519–4529.
856      https://doi.org/https://doi.org/10.1016/j.atmosenv.2004.05.032
857  Mahowald, N. (2011). Aerosol Indirect Effect on Biogeochemical Cycles and Climate. *Science*,
858      *334*(6057), 794–796. https://doi.org/10.1126/science.1207374
859  Metzger, S., Mihalopoulos, N., & Lelieveld, J. (2006). Importance of mineral cations and
860      organics in gas-aerosol partitioning of reactive nitrogen compounds: case study based on
861      MINOS results. *Atmospheric Chemistry and Physics*, *6*(9), 2549–2567.
862      https://doi.org/10.5194/acp-6-2549-2006
863  Myhre, G., & Stordal, F. (2001). Global sensitivity experiment of the radiative forcing due to
864      mineral aerosols. *Journal of Geophysical Research*, *106*, 18193–18204.
865      https://doi.org/10.1029/2000JD900536
866  Nenes, A., Krom, M. D., Mihalopoulos, N., Van Cappellen, P., Shi, Z., Bougiatioti, A., Zarmpas,
867      P., & Herut, B. (2011). Atmospheric acidification of mineral aerosols: a source of
868      bioavailable phosphorus for the oceans. *Atmospheric Chemistry and Physics*, *11*(13), 6265–
869      6272. https://doi.org/10.5194/acp-11-6265-2011
870  Olson, N.E., May, N.W., Kirpes, R.M., Watson, A.E., Hajny, K.D., Slade, J.H., Shepson, P.B.,
871      Stirm, B.H., Pratt, K.A., & Ault, A.P. (2019) Lake spray aerosol incorporated into Great
872      Lakes Clouds. *ACS Earth & Space Chemistry*, *3*, (12), 2765-2774.
873  Pringle, K. J., Tost, H., Pozzer, A., Pöschl, U., & Lelieveld, J. (2010). Global distribution of the
874      effective aerosol hygroscopicity parameter for CCN activation. *Atmospheric Chemistry and*
875      *Physics*, *10*(12), 5241–5255. https://doi.org/10.5194/acp-10-5241-2010
876  Prospero, J M. (1968). atmospheric dust studies on Barbados. *Bulletin of the American*
877      *Meteorological Society*, *49*(6), 645–652. https://doi.org/10.1175/1520-0477-49.6.645
878  Prospero, J. M., & Mayol-Bracero, O. L. (2013). Understanding the transport and impact of
879      African dust on the Caribbean Basin. *Bulletin of the American Meteorological Society*,
880      *94*(9), 1329–1337. https://doi.org/10.1175/BAMS-D-12-00142.1
881  Prospero, J. M. (1999). Long-range transport of mineral dust in the global atmosphere: Impact of
882      African dust on the environment of the southeastern United States. *Proceedings of the*
883      *National Academy of Sciences*, *96*(7), 3396 LP – 3403.
884      https://doi.org/10.1073/pnas.96.7.3396
885  Prospero, J.M, Blades, E., Mathison, G., & Naidu, R. (2005). Interhemispheric transport of
886      viable fungi and bacteria from Africa to the Caribbean with soil dust. *Aerobiologia*, *21*(1),
887      1–19. https://doi.org/10.1007/s10453-004-5872-7
888  Prospero, J. M, Delany, A. C., Delany, A. C., & Carlson, T. N. (2021). The Discovery of African
889      Dust Transport to the Western Hemisphere and the Saharan Air Layer: A History. *Bulletin*
890      *of the American Meteorological Society*, *102*(6), E1239–E1260.

891    https://doi.org/10.1175/BAMS-D-19-0309.1

892  Quinn, P. K., Thompson, E. J., Coffman, D. J., Baidar, S., Bariteau, L., Bates, T. S., Bigorre, S.,
893    Brewer, A., de Boer, G., de Szoeke, S. P., Drushka, K., Foltz, G. R., Intrieri, J., Iyer, S.,
894    Fairall, C. W., Gaston, C. J., Jansen, F., Johnson, J. E., Krüger, O. O., Marchbanks, R. D.,
895    Moran, K. P., Noone, D., Pezoa, S., Pincus, R., Plueddemann, A. J., Pöhlker, M. L., Pöschl,
896    U., Quinones Melendez, E., Royer, H. M., Szczodrak, M., Thomson, J., Upchurch, L. M.,
897    Zhang, C., Zhang, D., & Zuidema, P. (2021). Measurements from the RV Ronald H. Brown
898    and related platforms as part of the Atlantic Tradewind Ocean-Atmosphere Mesoscale
899    Interaction Campaign (ATOMIC). *Earth Syst. Sci. Data*, *13*(4), 1759–1790.
900    https://doi.org/10.5194/essd-13-1759-2021

901  Rickly, P. S., Guo, H., Campuzano-Jost, P., Jimenez, J. L., Wolfe, G. M., Bennett, R., Bourgeois,
902    I., Crounse, J. D., Dibb, J. E., DiGangi, J. P., Diskin, G. S., Dollner, M., Gargulinski, E. M.,
903    Hall, S. R., Halliday, H. S., Hanisco, T. F., Hannun, R. A., Liao, J., Moore, R., Nault, B. A.,
904    Nowak, J. B., Peischl, J., Robinson, C. E., Ryerson, T., Sanchez, K. J., Schöberl, M., Soja,
905    A. J., St. Clair, J. M., Thornhill, K. L., Ullmann, K., Wennberg, P. O., Weinzierl, B.,
906    Wiggins, E. B., Winstead, E. L., & Rollins, A. W. (2022). Emission factors and evolution of
907    $SO_2$ measured from biomass burning in wildfires and agricultural fires. *Atmospheric
908    Chemistry and Physics*, *22*(23), 15603–15620. https://doi.org/10.5194/acp-22-15603-2022

909  Rodriguez, S., Alastuey, A., Alonso-Pérez, S., Querol, X., Cuevas, E., Abreu-Afonso, J., Viana,
910    M., Pérez, N., Pandolfi, M., & de la Rosa, J. (2011). Transport of desert dust mixed with
911    North African industrial pollutants in the subtropical Saharan Air Layer. *Atmospheric
912    Chemistry & Physics*, *11*, 6663-6685.

913  Rodríguez, S., Prospero, J.M., López-Darias, J., García-Alvarez, M.-I., Zuidema, P., Nava, S.,
914    Lucarelli, F., Gaston, C.J., Galindo, L., & Sosa, E. (2021). Tracking the changes of iron
915    solubility and air pollutants traces as African dust transits the Atlantic in the Saharan dust
916    outbreaks. *Atmospheric Environment*, *246*, https://doi.org/10.1016/j.atmosenv.2020.118092.

917  Rosenfeld, D., Rudich, Y., & Lahav, R. (2001). Desert dust suppressing precipitation: A possible
918    desertification feedback loop. *Proceedings of the National Academy of Sciences*, *98*(11),
919    5975 LP – 5980. https://doi.org/10.1073/pnas.101122798

920  Royer, H. M., Pöhlker, M. L., Krüger, O., Blades, E., Sealy, P., Lata, N. N., Cheng, Z., China, S.,
921    Ault, A. P., Quinn, P. K., Zuidema, P., Pöhlker, C., Pöschl, U., Andreae, M., & Gaston, C.
922    J. (2023). African smoke particles act as cloud condensation nuclei in the wintertime
923    tropical North Atlantic boundary layer over Barbados. *Atmospheric Chemistry and Physics*,
924    *23*(2), 981–998. https://doi.org/10.5194/acp-23-981-2023

925  Ryder, C. L., Marenco, F., Brooke, J. K., Estelles, V., Cotton, R., Formenti, P., McQuaid, J. B.,
926    Price, H. C., Liu, D., Ausset, P., Rosenberg, P. D., Taylor, J. W., Choularton, T., Bower, K.,
927    Coe, H., Gallagher, M., Crosier, J., Lloyd, G., Highwood, E. J., & Murray, B. J. (2018).
928    Coarse-mode mineral dust size distributions, composition and optical properties from AER-
929    D aircraft measurements over the tropical eastern Atlantic. *Atmospheric Chemistry and
930    Physics*, *18*(23), 17225–17257. https://doi.org/10.5194/acp-18-17225-2018

931  Savoie, D L, & Prospero, J. M. (1982). Particle size distribution of nitrate and sulfate in the
932    marine atmosphere. *Geophysical Research Letters*, *9*(10), 1207–1210.
933    https://doi.org/https://doi.org/10.1029/GL009i010p01207

934  Savoie, Dennis L, Arimoto, R., Keene, W. C., Prospero, J. M., Duce, R. A., & Galloway, J. N.
935    (2002). Marine biogenic and anthropogenic contributions to non-sea-salt sulfate in the
936    marine boundary layer over the North Atlantic Ocean. *Journal of Geophysical Research:*

*Atmospheres*, *107*(D18), AAC 3-1-AAC 3-21.
https://doi.org/https://doi.org/10.1029/2001JD000970

Shen, H., Peters, T. M., Casuccio, G. S., Lersch, T. L., West, R. R., Kumar, A., Kumar, N., & Ault, A. P. (2016). Elevated Concentrations of Lead in Particulate Matter on the Neighborhood-Scale in Delhi, India As Determined by Single Particle Analysis. *Environmental Science & Technology*, *50*(10), 4961–4970. https://doi.org/10.1021/acs.est.5b06202

Shi, Z., Zhang, D., Hayashi, M., Ogata, H., Ji, H., & Fujiie, W. (2008). Influences of sulfate and nitrate on the hygroscopic behaviour of coarse dust particles. *Atmospheric Environment*, *42*(4), 822–827. https://doi.org/https://doi.org/10.1016/j.atmosenv.2007.10.037

Sobanska, S., Coeur, C., Maenhaut, W., & Adams, F. (2003). SEM-EDX Characterisation of Tropospheric Aerosols in the Negev Desert (Israel). *Journal of Atmospheric Chemistry*, *44*(3), 299–322. https://doi.org/10.1023/A:1022969302107

Sokolik, I. N., Winker, D. M., Bergametti, G., Gillette, D. A., Carmichael, G., Kaufman, Y. J., Gomes, L., Schuetz, L., & Penner, J. E. (2001). Introduction to special section: Outstanding problems in quantifying the radiative impacts of mineral dust. *Journal of Geophysical Research: Atmospheres*, *106*(D16), 18015–18027. https://doi.org/https://doi.org/10.1029/2000JD900498

Spokes, L. J., & Jickells, T. D. (1995). Factors controlling the solubility of aerosol trace metals in the atmosphere and on mixing into seawater. *Aquatic Geochemistry*, *1*(4), 355–374. https://doi.org/10.1007/BF00702739

Stein, A.F., Draxler, R.R., Rolph, G.D., Stunder, B.J.B., Cohen, M.D., & Ngan, F. (2015). NOAA's HYSPLIT atmospheric transport and dispersion modeling system. *Bulletin of the American Meteorological Society*, *96*(12), 2059-2077.

Stevens, B., Bony, S., Farrell, D., Ament, F., Blyth, A., Fairall, C., Karstensen, J., Quinn, P. K., Speich, S., Acquistapace, C., Aemisegger, F., Albright, A. L., Bellenger, H., Bodenschatz, E., Caesar, K.-A., Chewitt-Lucas, R., de Boer, G., Delanoë, J., Denby, L., Ewald, F., Fildier, B., Forde, M., George, G., Gross, S., Hagen, M., Hausold, A., Heywood, K. J., Hirsch, L., Jacob, M., Jansen, F., Kinne, S., Klocke, D., Kölling, T., Konow, H., Lothon, M., Mohr, W., Naumann, A. K., Nuijens, L., Olivier, L., Pincus, R., Pöhlker, M., Reverdin, G., Roberts, G., Schnitt, S., Schulz, H., Siebesma, A. P., Stephan, C. C., Sullivan, P., Touzé-Peiffer, L., Vial, J., Vogel, R., Zuidema, P., Alexander, N., Alves, L., Arixi, S., Asmath, H., Bagheri, G., Baier, K., Bailey, A., Baranowski, D., Baron, A., Barrau, S., Barrett, P. A., Batier, F., Behrendt, A., Bendinger, A., Beucher, F., Bigorre, S., Blades, E., Blossey, P., Bock, O., Böing, S., Bosser, P., Bourras, D., Bouruet-Aubertot, P., Bower, K., Branellec, P., Branger, H., Brennek, M., Brewer, A., Brilouet, P.-E., Brügmann, B., Buehler, S. A., Burke, E., Burton, R., Calmer, R., Canonici, J.-C., Carton, X., Cato Jr., G., Charles, J. A., Chazette, P., Chen, Y., Chilinski, M. T., Choularton, T., Chuang, P., Clarke, S., Coe, H., Cornet, C., Coutris, P., Couvreux, F., Crewell, S., Cronin, T., Cui, Z., Cuypers, Y., Daley, A., Damerell, G. M., Dauhut, T., Deneke, H., Desbios, J.-P., Dörner, S., Donner, S., Douet, V., Drushka, K., Dütsch, M., Ehrlich, A., Emanuel, K., Emmanouilidis, A., Etienne, J.-C., Etienne-Leblanc, S., Faure, G., Feingold, G., Ferrero, L., Fix, A., Flamant, C., Flatau, P. J., Foltz, G. R., Forster, L., Furtuna, I., Gadian, A., Galewsky, J., Gallagher, M., Gallimore, P., Gaston, C., Gentemann, C., Geyskens, N., Giez, A., Gollop, J., Gouirand, I., Gourbeyre, C., de Graaf, D., de Groot, G. E., Grosz, R., Güttler, J., Gutleben, M., Hall, K., Harris, G., Helfer, K. C., Henze, D., Herbert, C., Holanda, B., Ibanez-Landeta, A.,

Intrieri, J., Iyer, S., Julien, F., Kalesse, H., Kazil, J., Kellman, A., Kidane, A. T., Kirchner, U., Klingebiel, M., Körner, M., Kremper, L. A., Kretzschmar, J., Krüger, O., Kumala, W., Kurz, A., L'Hégaret, P., Labaste, M., Lachlan-Cope, T., Laing, A., Landschützer, P., Lang, T., Lange, D., Lange, I., Laplace, C., Lavik, G., Laxenaire, R., Le Bihan, C., Leandro, M., Lefevre, N., Lena, M., Lenschow, D., Li, Q., Lloyd, G., Los, S., Losi, N., Lovell, O., Luneau, C., Makuch, P., Malinowski, S., Manta, G., Marinou, E., Marsden, N., Masson, S., Maury, N., Mayer, B., Mayers-Als, M., Mazel, C., McGeary, W., McWilliams, J. C., Mech, M., Mehlmann, M., Meroni, A. N., Mieslinger, T., Minikin, A., Minnett, P., Möller, G., Morfa Avalos, Y., Muller, C., Musat, I., Napoli, A., Neuberger, A., Noisel, C., Noone, D., Nordsiek, F., Nowak, J. L., Oswald, L., Parker, D. J., Peck, C., Person, R., Philippi, M., Plueddemann, A., Pöhlker, C., Pörtge, V., Pöschl, U., Pologne, L., Posyniak, M., Prange, M., Quiñones Meléndez, E., Radtke, J., Ramage, K., Reimann, J., Renault, L., Reus, K., Reyes, A., Ribbe, J., Ringel, M., Ritschel, M., Rocha, C. B., Rochetin, N., Röttenbacher, J., Rollo, C., Royer, H., Sadoulet, P., Saffin, L., Sandiford, S., Sandu, I., Schäfer, M., Schemann, V., Schirmacher, I., Schlenczek, O., Schmidt, J., Schröder, M., Schwarzenboeck, A., Sealy, A., Senff, C. J., Serikov, I., Shohan, S., Siddle, E., Smirnov, A., Späth, F., Spooner, B., Stolla, M. K., Szkółka, W., de Szoeke, S. P., Tarot, S., Tetoni, E., Thompson, E., Thomson, J., Tomassini, L., Totems, J., Ubele, A. A., Villiger, L., von Arx, J., Wagner, T., Walther, A., Webber, B., Wendisch, M., Whitehall, S., Wiltshire, A., Wing, A. A., Wirth, M., Wiskandt, J., Wolf, K., Worbes, L., Wright, E., Wulfmeyer, V., Young, S., Zhang, C., Zhang, D., Ziemen, F., Zinner, T., & Zöger, M. (2021). EUREC4A. *Earth Syst. Sci. Data*, *13*(8), 4067–4119. https://doi.org/10.5194/essd-13-4067-2021

Stockdale, A., Krom, M. D., Mortimer, R. J. G., Benning, L. G., Carslaw, K. S., Herbert, R. J., Shi, Z., Myriokefalitakis, S., Kanakidou, M., & Nenes, A. (2016). Understanding the nature of atmospheric acid processing of mineral dusts in supplying bioavailable phosphorus to the oceans. *Proceedings of the National Academy of Sciences*, *113*(51), 14639–14644. https://doi.org/10.1073/pnas.1608136113

Sullivan, R. C., Guazzotti, S. A., Sodeman, D. A., & Prather, K. A. (2007). Direct observations of the atmospheric processing of Asian mineral dust. *Atmospheric Chemistry and Physics*, *7*(5), 1213–1236. https://doi.org/10.5194/acp-7-1213-2007

Sullivan, R. C., Moore, M. J. K., Petters, M. D., Kreidenweis, S. M., Roberts, G. C., & Prather, K. A. (2009). Effect of chemical mixing state on the hygroscopicity and cloud nucleation properties of calcium mineral dust particles. *Atmospheric Chemistry and Physics*, *9*(10), 3303–3316. https://doi.org/10.5194/acp-9-3303-2009

Sullivan, R. C., & Prather, K. A. (2007). Investigations of the diurnal cycle and mixing state of oxalic acid in individual particles in Asian aerosol outflow. *Environmental Science and Technology*, *41*(23), 8062–8069. https://doi.org/10.1021/es071134g

Tang, M. J., Cziczo, D. J., and Grassian, V. H. (2016) Interactions of water with mineral dust aerosol: Water adsorption, hygroscopicity, cloud condensation and ice nucleation. *Chemical Reviews*, 116, 4205–4259.

Tegen, I. (2003). Modeling the mineral dust aerosol cycle in the climate system. *Quaternary Science Reviews*, *22*(18), 1821–1834. https://doi.org/https://doi.org/10.1016/S0277-3791(03)00163-X

Tsamalis, C., Chédin, A., Pelon, J., & Capelle, V. (2013). The seasonal vertical distribution of the Saharan Air Layer and its modulation by the wind. *Atmos. Chem. Phys.*, *13*(22), 11235–11257. https://doi.org/10.5194/acp-13-11235-2013

Ullerstam, M., Vogt, R., Langer, S., & Ljungström, E. (2002). The kinetics and mechanism of SO2 oxidation by O3 on mineral dust. *Physical Chemistry Chemical Physics*, *4*(19), 4694–4699. https://doi.org/10.1039/B203529B

van Herpen, M.M.J.W., Li, Q., Saiz-Lopez, A., Liisberg, J.B., Röckmann, T., Cuevas, C.A., Fernandez, R.P., Mak, J.E., Mahowald, N.M., Hess, P., Meidan, D., Stuut, J.-B.W., & Johnson, M.S. (2023). Photocatalytic chlorine atom production on mineral dust-sea spray aerosols over the North Atlantic. *Proceedings of the National Academy of Sciences*, *120*(31), https://doi.org/10.1073/pnas.2303974120.

Weinzierl, B., Ansmann, A., Prospero, J. M., Althausen, D., Benker, N., Chouza, F., Dollner, M., Farrell, D., Fomba, W. K., Freudenthaler, V., Gasteiger, J., Groß, S., Haarig, M., Heinold, B., Kandler, K., Kristensen, T. B., Mayol-Bracero, O. L., Müller, T., Reitebuch, O., Sauer, D., Schäfler, A., Schepanski, K., Spanu, A., Tegen, I., Toledano, C., & Walser, A. (2017). The Saharan Aerosol Long-Range Transport and Aerosol–Cloud-Interaction Experiment: Overview and Selected Highlights. *Bulletin of the American Meteorological Society*, *98*(7), 1427–1451. https://doi.org/https://doi.org/10.1175/BAMS-D-15-00142.1

Wu, Z., Birmili, W., Poulain, L., Wang, Z., Merkel, M., Fahlbusch, B., van Pinxteren, D., Herrmann, H., & Wiedensohler, A. (2013). Particle hygroscopicity during atmospheric new particle formation events: implications for the chemical species contributing to particle growth. *Atmospheric Chemistry and Physics*, *13*(13), 6637–6646. https://doi.org/10.5194/acp-13-6637-2013

Wurzler, S., Reisin, T. G., & Levin, Z. (2000). Modification of mineral dust particles by cloud processing and subsequent effects on drop size distributions. *Journal of Geophysical Research: Atmospheres*, *105*(D4), 4501–4512. https://doi.org/https://doi.org/10.1029/1999JD900980

Zhang, H.H., Li, R., Huang, C.P., Li, X.F., Dong, S.W., Wang, F., Li, T.T., Chen, Y.Z., Zhang, G.H., Ren, Y., Chen, Q.C., Huang, R.J., Chen, S.Y., Xue, T., Wang, X.M., & Tang, M.J. (2023) Seasonal variation of aerosol iron solubility in coarse and fine particles at an inland city in northwestern China. *Atmospheric Chemistry & Physics*, *23*, 3543-3559.

Zuidema, P., Alvarez, C., Kramer, S. J., Custals, L., Izaguirre, M., Sealy, P., Prospero, J. M., & Blades, E. (2019). Is Summer African Dust Arriving Earlier to Barbados? The Updated Long-Term In Situ Dust Mass Concentration Time Series from Ragged Point, Barbados, and Miami, Florida. *Bulletin of the American Meteorological Society*, *100*(10), 1981–1986. https://doi.org/10.1175/BAMS-D-18-0083.1